

154

LEVEL

10

AD-E300787

DNA 4839F

ADA 085581

NUCLEAR AIRBLAST SIMULATION USING FUEL-AIR EXPLOSIVES

H-Tech Laboratories, Inc.
P.O. Box 1686
Santa Monica, California 90406

31 December 1978

Final Report for Period December 1976—December 1978

CONTRACT No. DNA 001-77-C-0101

APPROVED FOR PUBLIC RELEASE;
DISTRIBUTION UNLIMITED.

DTIC
REFLECTE
JUN 18 1980

C

THIS WORK SPONSORED BY THE DEFENSE NUCLEAR AGENCY
UNDER RDT&E RMSS CODE B344077464 Y99QAXSD07032 H2590D.

Prepared for
Director
DEFENSE NUCLEAR AGENCY
Washington, D. C. 20305

DDC FILE COPY.

80 5 7 030

Destroy this report when it is no longer needed. Do not return to sender.

PLEASE NOTIFY THE DEFENSE NUCLEAR AGENCY,
ATTN: STTI, WASHINGTON, D.C. 20305, IF
YOUR ADDRESS IS INCORRECT, IF YOU WISH TO
BE DELETED FROM THE DISTRIBUTION LIST, OR
IF THE ADDRESSEE IS NO LONGER EMPLOYED BY
YOUR ORGANIZATION.



UNCLASSIFIED

SECURITY CLASSIFICATION OF THIS PAGE (When Data Entered)

REPORT DOCUMENTATION PAGE		READ INSTRUCTIONS BEFORE COMPLETING FORM
1. REPORT NUMBER DNA 4839F	2. GOVT ACCESSION NO. AD-A085581	3. RECIPIENT'S CATALOG NUMBER
4. TITLE (and Subtitle) NUCLEAR AIRBLAST SIMULATION USING FUEL-AIR EXPLOSIVES		5. TYPE OF REPORT & PERIOD COVERED Final Report for Period Dec 76—Dec 78
		6. PERFORMING ORG. REPORT NUMBER
7. AUTHOR(s) B. A. Hartenbaum		8. CONTRACT OR GRANT NUMBER(s) DNA 001-77-C-0101
9. PERFORMING ORGANIZATION NAME AND ADDRESS H-Tech Laboratories, Inc. P.O. Box 1686 Santa Monica, California 90406		10. PROGRAM ELEMENT, PROJECT, TASK AREA & WORK UNIT NUMBERS Subtask Y99QAXSD070-32
11. CONTROLLING OFFICE NAME AND ADDRESS Director Defense Nuclear Agency Washington, D.C. 20305		12. REPORT DATE 31 December 1978
		13. NUMBER OF PAGES 68
14. MONITORING AGENCY NAME & ADDRESS (if different from Controlling Office)		15. SECURITY CLASS (of this report) UNCLASSIFIED
		15a. DECLASSIFICATION/DOWNGRADING SCHEDULE
16. DISTRIBUTION STATEMENT (of this Report) Approved for public release; distribution unlimited.		
17. DISTRIBUTION STATEMENT (of the abstract entered in Block 20, if different from Report)		
18. SUPPLEMENTARY NOTES This work sponsored by the Defense Nuclear Agency under RDT&E RMSS Code B344077464 Y99QAXSD07032 H2590D.		
19. KEY WORDS (Continue on reverse side if necessary and identify by block number) Airblast Simulator Fuel-Air Explosives Nuclear Weapons Effects		
20. ABSTRACT (Continue on reverse side if necessary and identify by block number) Airblast effects and airblast simulation at overpressures less than 100 psig are reviewed and the use of fuel-air mixtures as an explosive driver for a nuclear airblast simulator is evaluated. Methods for dispersing fuel are presented and estimates are made on the use of fluid jets to create explosive fuel-air mixtures. Calculations are made of the reach, dispersion, and detonability of long range fuel jets. Experimental fuel-air data are analyzed. It is concluded that small-scale experiments have demonstrated		

UNCLASSIFIED

SECURITY CLASSIFICATION OF THIS PAGE(When Data Entered)

20. ABSTRACT (Continued)

the feasibility of using liquid jets to create a hemispherical detonable cloud (at least in the small), but that scaling to 1 KT from 1/4 ton experiments is very uncertain. Intermediate-scale experiments appear necessary. Simulator criteria are reviewed. Certain issues involving underwater shock and ground shock in addition to airblast are clarified.

UNCLASSIFIED

SECURITY CLASSIFICATION OF THIS PAGE(When Data Entered)

PREFACE

This work was sponsored by the Defense Nuclear Agency under Government Contract No. DNA001-77-C-0101 and was authorized under Project Y99QAXS, Task D070, Work Unit 32. The DNA Contracting Officer's Representatives were Major George Goss and Commander Thomas J. Deevy. It is the author's pleasure to acknowledge many helpful technical discussions with Bradford Sturtevant and Julian Cole, especially on the subject of fluid jet propagation. The author is indebted to William Benedick of Sandia Laboratories, Albuquerque for a detailed review of the Sandia studies on fuel-air explosions.

Accession For	
NTIS GRA&I	<input checked="" type="checkbox"/>
DDC TAB	<input type="checkbox"/>
Unannounced	<input type="checkbox"/>
Justification	<input type="checkbox"/>
By	
Distribution/	
Availability Codes	
Dist	Avail and/or special
A	

CONVERSION FACTORS

To Convert From	To	Multiply By
angstrom	meters (m)	1.000 000 X E -10
atmosphere (normal)	kilo pascal (kPa)	1.013 25 X E +2
bar	kilo pascal (kPa)	1.000 000 X E +2
barn	meter ² (m ²)	1.000 000 X E -28
British thermal unit (thermochemical)	joule (J)	1.054 350 X E +3
calorie (thermochemical)	joule (J)	4.184 000
cal (thermochemical)/cm ²	mega joule/m ² (MJ/m ²)	4.184 000 X E -2
curie	giga becquerel (GBq)*	3.700 000 X E +1
degree (angle)	radian (rad)	1.745 329 X E -2
degree Fahrenheit	degree kelvin (K)	$T_K = (T_F + 459.67)/1.8$
electron volt	joule (J)	1.602 19 X E -19
erg	joule (J)	1.000 000 X E -7
erg/second	watt (W)	1.000 000 X E -7
foot	meter (m)	3.048 000 X E -1
foot-pound-force	joule (J)	1.355 818
gallon (U.S. liquid)	meter ³ (m ³)	3.785 412 X E -3
inch	meter (m)	2.540 000 X E -2
jerk	joule (J)	1.000 000 X E +9
joule/kilogram (J/kg) (radiation dose absorbed)	Gray (Gy)**	1.000 000
kilotons	terajoules	4.183
kip (1000 lbf)	newton (N)	4.448 222 X E +3
kip/inch ² (ksi)	kilo pascal (kPa)	6.894 757 X E +3
krad	newton-second/m ² (N-s/m ²)	1.000 000 X E +2
micron	meter (m)	1.000 000 X E -6
mil	meter (m)	2.540 000 X E -5
mile (international)	meter (m)	1.609 344 X E +3
ounce	kilogram (kg)	2.834 952 X E -2
pound-force (lbf avoirdupois)	newton (N)	4.448 222
pound-force inch	newton-meter (N·m)	1.129 848 X E -1
pound-force/inch	newton/meter (N/m)	1.751 268 X E +2
pound-force/foot ²	kilo pascal (kPa)	4.788 026 X E -2
pound-force/inch ² (psi)	kilo pascal (kPa)	6.894 757
pound-mass (lbm avoirdupois)	kilogram (kg)	4.535 924 X E -1
pound-mass-foot ² (moment of inertia)	kilogram-meter ² (kg·m ²)	4.214 011 X E -2
pound-mass/foot ³	kilogram/meter ³ (kg/m ³)	1.601 846 X E +1
rad (radiation dose absorbed)	Gray (Gy)**	1.000 000 X E -2
roentgen	coulomb/kilogram (C/kg)	2.579 760 X E -4
shake	second (s)	1.000 000 X E -8
slug	kilogram (kg)	1.459 390 X E +1
torr (mm Hg, 0° C)	kilo pascal (kPa)	1.333 22 X E -1

*The becquerel (Bq) is the SI unit of radioactivity; 1 Bq = 1 event/s.
 **The Gray (Gy) is the SI unit of absorbed radiation.

A more complete listing of conversions may be found in "Metric Practice Guide E 380-74," American Society for Testing and Materials.

TABLE OF CONTENTS

Section	Page
1	INTRODUCTION AND SUMMARY - - - - - 5
1.1	GENERAL CONSIDERATIONS - - - - - 5
1.2	SUMMARY OF PRINCIPAL RESULTS - - - - - 6
2	NUCLEAR AIRBLAST SIMULATION USING FUEL-AIR EXPLOSIVES - - - 8
2.1	GENERAL REMARKS- - - - - 8
2.2	BLAST EFFECTS INDUCED BY FUEL-AIR, GASEOUS AND CONDENSED EXPLOSIVES - - - - - 8
3	FUEL DISPERSAL AND DETONATION - - - - - 21
3.1	FUEL DISPERSAL TECHNIQUES - - - - - 21
3.2	BOIL-OFF - - - - - 21
3.3	EXPLOSIVE DISSEMINATION - - - - - 22
3.4	LIQUID JET PROPAGATION AND DISPERSAL - - - - - 22
3.4.1	Jet Design - - - - - 22
3.4.2	Detonability and Types of Fuels - - - - - 29
3.4.3	Experimental Data - - - - - 32
3.5	WIND EFFECTS - - - - - 32
3.6	TEST PROGRAM AND INSTRUMENTATION - - - - - 34
4	THE EXPERIMENTAL PROGRAM - - - - - 35
4.1	PROGRAM GUIDELINES - - - - - 35
4.2	REVIEW OF EXPERIMENTAL FAE DETONATION AND JET PROPAGATION DATA - - - - - 35
5	PRELIMINARY SPECIFICATIONS FOR NUCLEAR BLAST AND SHOCK SIMULATORS - - - - - 43
5.1	SIMULATION CRITERIA - - - - - 43
5.2	NUCLEAR UNDERWATER SHOCK EFFECTS - - - - - 44
5.3	NUCLEAR AIRBLAST EFFECTS - - - - - 47
5.4	DEEP BASED STRUCTURES - - - - - 51
5.5	SHALLOW BURIED STRUCTURES - - - - - 52
6	CONCLUSIONS AND RECOMMENDATIONS - - - - - 54
7	REFERENCES - - - - - 56
Appendix	
A	NOMENCLATURE - - - - - 59
B	OVERPRESSURE WAVEFORMS - - - - - 61

LIST OF ILLUSTRATIONS

<u>Figure</u>		<u>Page</u>
2.1	Peak static overpressure vs. range for nuclear and gaseous surface explosions - - - - -	9
2.2	Peak static overpressure vs. range for nuclear, TNT, and methane-oxygen explosions - - - - -	10
2.3	Propane-oxygen surface burst peak pressure - - - - -	13
2.4	Propane-oxygen positive phase static overpressure impulse data - - - - -	14
2.5	Propane-oxygen waveform (BRL) vs. the nuclear waveform - - -	16
2.6	TNT overpressure waveform (AFWL) vs. the nuclear waveform -	17
2.7	TNT overpressure waveform (AFWL) vs. the nuclear waveform -	18
2.8	Propane-oxygen waveform (BRL) vs. nuclear waveform - - - - -	19
3.1	Calculated propagation of turbulent liquid jets in air - - -	26
3.2	Calculated liquid phase mass concentration - - - - -	28
3.3	Fuel mass concentration in jets - - - - -	31
3.4	Water jet (fire stream) data - - - - -	33
4.1	FAE positive phase overpressure impulse data (S^3) - - - - -	38
4.2	FAE peak overpressure data (S^3) - - - - -	40
5.1	The areal energy density in a simulator overpressure wave -	46
5.2	Thermal fluence vs. overpressure - - - - -	48
5.3	Range vs. overpressure for surface bursts - - - - -	50

LIST OF TABLES

<u>Table</u>		<u>Page</u>
4.1	Program guidelines. Unknowns and parameters - - - - -	36
4.2	Propylene oxide transient jet performance- - - - -	41
4.3	Single jet propagation and detonability scaling tests - - -	42

SECTION 1

INTRODUCTION AND SUMMARY

1.1 GENERAL CONSIDERATIONS

Operational and treaty obligations have dictated that non-nuclear means be used to test the response of structures to nuclear explosion induced airblast. TNT and more recently ANFO have been the principal explosives used to create an unconfined airblast. To eliminate cratering and the damage to test structures caused by ejecta arising from the use of solid explosives, and to increase the frequency of testing, the use of gaseous explosions was investigated a number of years ago. Although based on sound principles, the gaseous detonation program foundered in attempting to produce a practical system. The last series of tests carried out (1967) suffered both from the failure of the gas bag system and from premature ignition.

Stimulated by the need for improved airblast testing and encouraged by the military fuel-air explosives program, the Defense Nuclear Agency undertook a program to assess the feasibility of employing fuel-air mixtures as the explosive driver for an airblast test facility. The facility would be used for subjecting structures to overpressures between one and one-hundred psig arising from the simulated detonation of a one kiloton nuclear surface blast. It was postulated that the use of fuel-air explosives might result in several benefits to a test program which include the elimination of cratering, debris and jetting, a better match to the nuclear pressure vs. range curve than can be obtained with condensed explosives, a rapid experiment turn-around and lower cost. Whether these benefits can be realized depends upon the resolution of questions regarding detonability, fuel dispersal, uniformity of the explosive structure, wind effects, fuel selection and replication of nuclear waveforms.

The purpose of the work described in this report was to:

- (1) Provide an overview on the use of fuel-air explosions (called FAE) to simulate nuclear airblast.

- (2) Provide technical analyses on the dispersion of liquid fuel to create a detonable mixture,
- (3) Assist in the planning, design, analysis and evaluation of the results of an experimental program to determine the feasibility of using fuel-air explosions to simulate nuclear airblast between one and one-hundred psig, and
- (4) Clarify some design issues involving weapons effects simulators for airblast, underwater effects and ground shock.

A review of airblast effects and airblast simulation at overpressures less than one hundred psig is presented in Section 2, along with an overview on the use of fuel-air mixtures as an explosive driver for a nuclear airblast simulator. Methods for dispersing fuel and estimates on the use of fluid jets to create an explosive fuel-air mixture are presented in Section 3. Calculations are made on the reach, dispersion and detonability of long range fuel jets. Measurements taken by Systems, Science and Software of overpressures arising from the detonation of small-scale (30 foot diameter) propylene oxide hemispherical charges formed by the action of fluid jets are reviewed in Section 4. Some general considerations of blast simulators involving air shock, underwater explosions and ground shock are presented in Section 5.

1.2 SUMMARY OF PRINCIPAL RESULTS

A critical review of airblast phenomena has revealed that an evaluation of an airblast simulator must be made on the basis of overpressure waveforms and analyses of drag loading. The nuclear blast overpressure vs. range curve cannot be duplicated by a chemical explosion over a wide range of pressures, although a close fit may be made over a very limited pressure range. Based upon the curvature of the pressure vs. range relation a better fit to the nuclear curve may be effected by a gaseous or fuel-air explosive than by a solid explosive.

Supported by previous simulator work, it is believed that the chief element of a good fuel-air program must be the accurate measurement of overpressure waveforms for comparison with nuclear waveforms. Accurate

calculations are necessary to assist in determining if departures of the fuel-air waveforms from nuclear waveforms are intrinsic to chemical explosions or arise from non-ideal detonations. Thorough calibration of the step response of gages is necessary to rule out instrumental errors. Analyses of drag loading are also required.

The theory of Abramovich predicts the long range propagation of liquid fuel jets and the creation of a detonable mixture (via air entrainment) at a jet length-to-diameter ratio of approximately 1000. Although the theory is the best that is available, it is believed that it would be remarkable if the calculations were accurate even to within an order of magnitude. Long range jet propagation and dispersion experiments are necessary.

Small-scale experiments have demonstrated the feasibility of using liquid jets to create a detonable cloud (at least in the small), but the similarity between the low pressure blast effects produced by a fuel-air explosion and by a nuclear explosion remains to be determined. Devising a methodology for scaling-up the FAE experiments is hampered by the apparent lack of similitude in the propagation and dispersion of long-range fuel jets. Future jet experiments must not only determine jet detonability, but also scaling relationships.

The importance of establishing simulation criteria is stressed. Specification of the nuclear environment to be simulated and the accuracy with which that environment is known have a significant impact on simulator design. Design sophistication may be unwarranted and the use of bounding environments appears to be crucial.

Certain issues involving underwater shock, airblast, and ground shock simulators were clarified. The relation between weapon yield, overpressure level and energy density for an underwater shock simulator is mapped out. If a focusing device could be constructed then a modest amount of explosive could be used to simulate large weapon yields and overpressures.

SECTION 2

NUCLEAR AIRBLAST SIMULATION USING FUEL-AIR EXPLOSIVES

2.1 GENERAL REMARKS

The principal purpose of this section is to outline what can be expected of a fuel-air program whose main objective is to simulate nuclear airblast below 100 psig. Because the work described in this report is but a small part of a larger program an ancillary purpose of this section is to outline additional work that must be accomplished. In assessing the usefulness of fuel-air explosives recourse is made to nuclear airblast data and calculations, and to the results of past simulation experiments and computations. For the purposes of initial analyses of blast production it is assumed that an explosion of a homogeneous gas mixture is equivalent to that of an ideal fuel-air explosive in which all of the fuel reacts in the same manner.

2.2 BLAST EFFECTS INDUCED BY FUEL-AIR, GASEOUS AND CONDENSED EXPLOSIVES

Based on experimental data and extant calculations a blast wave originating from a chemical explosion cannot duplicate the decay of peak overpressure with distance characteristic of a nuclear explosion over a wide range of pressures. To illustrate this fact, experimental and theoretical peak pressure vs. distance curves for a propane-oxygen explosion [1,2,3] are compared with nuclear curves [4,5,6] in Figure 2.1. A similar comparison for TNT [7] is made in Figure 2.2. The nuclear data are fit by a curve known as the U.S. '59 curve. H. Brode's calculation of a nuclear explosion begins to fall below the U.S. '59 nuclear data starting at 30 psig. The AFWL calculation known as the "1 KT Standard" lies above the nuclear data starting at 4 psig. The differences between the nuclear curves are a source of controversy; for the purpose of the present work the U.S. '59 curve will be employed. Free-air nuclear data are replotted for a surface burst using $(2W)^{1/3}$ scaling rather than, say, $(1.6W)^{1/3}$ scaling and the yield is scaled to 25.4 tons to effect a best fit (using graphical techniques) with the propane oxygen data between 7 and 40 psig.

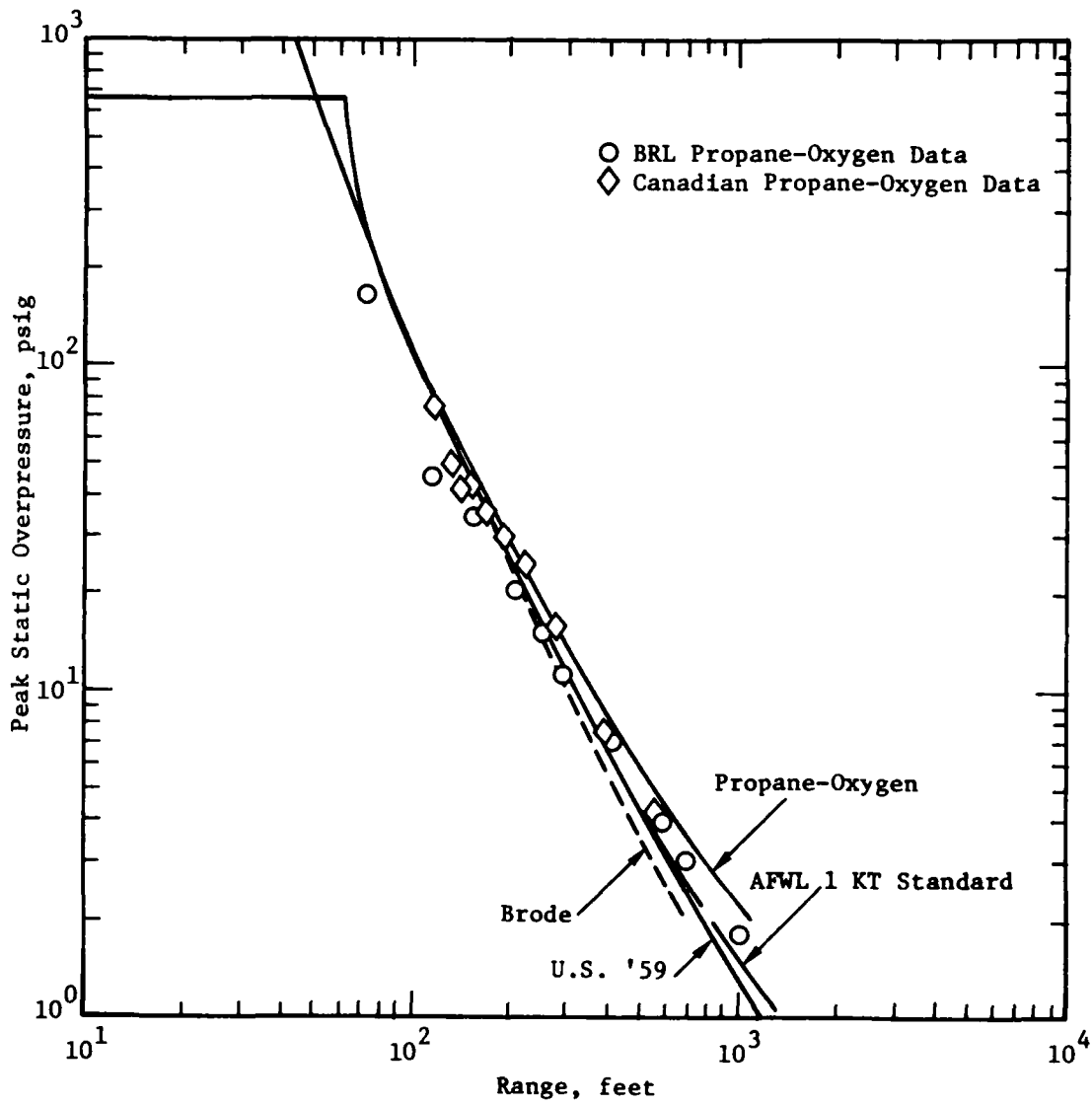


Figure 2.1 Peak static overpressure vs. range for nuclear and gaseous surface explosions. The U.S. '59 curve is a fit to experimental data scaled to 25.4 tons. The Brode and AFWL 1 KT Standard curves are based on time-marching computations. The propane-oxygen curve was calculated at General American Research Division. The propane-oxygen data were measured by the Ballistic Research Laboratory (BRL) and the Canadians on Operation Distant Plain

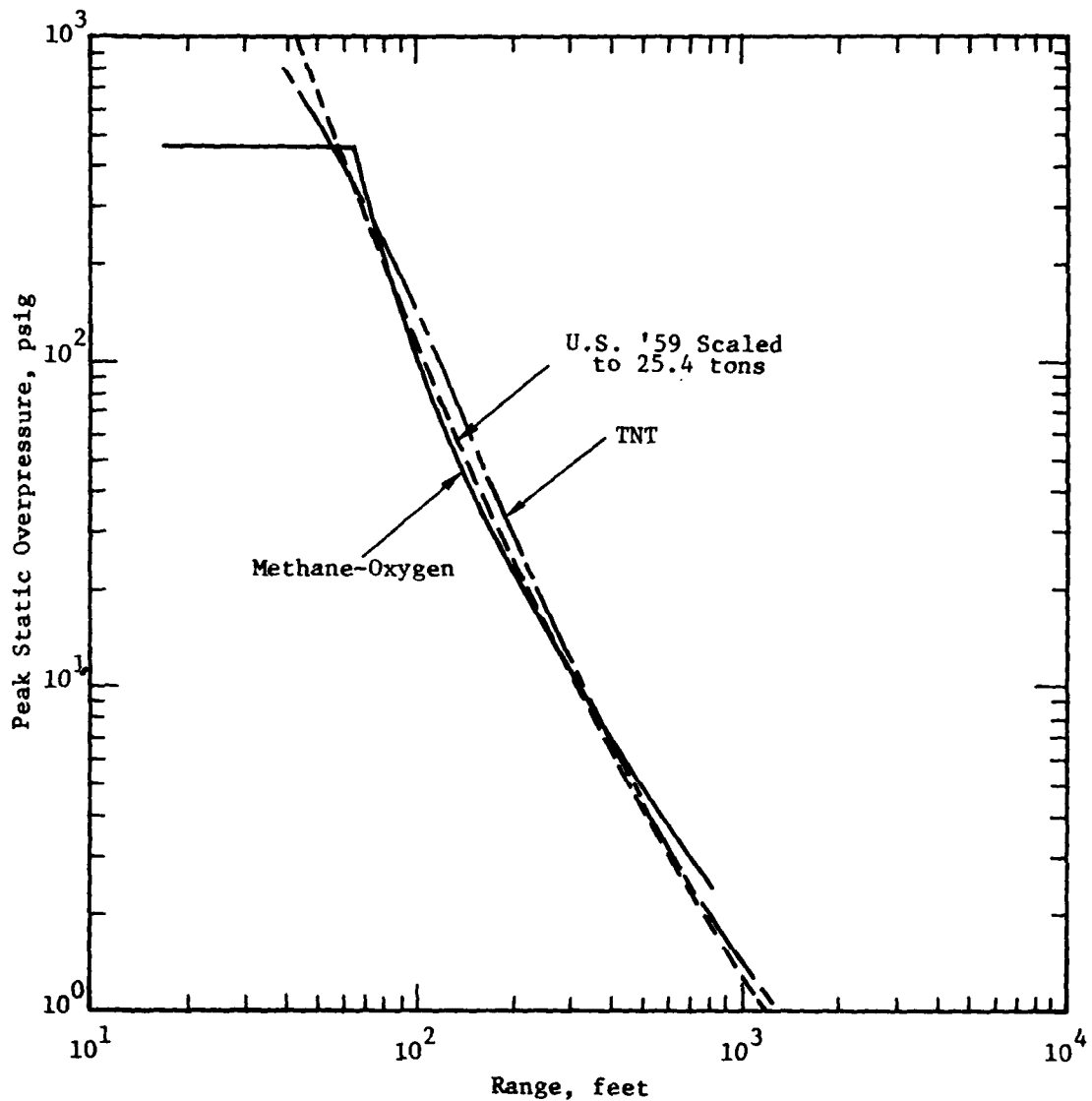


Figure 2.2 Peak static overpressure vs. range for nuclear, TNT, and methane-oxygen explosions. The nuclear and methane-oxygen curves exhibit positive curvature, but the TNT has negative curvature above 10 psig resulting in an offset between the nuclear and TNT curves. The nuclear curve is scaled to 25.4 tons from the 1 KT U.S. '59 curve. The methane-oxygen curve is scaled to 15 tons weight from a General American Research Division calculation. The TNT curve is scaled to 20 tons from a calculation by H. Brode.

The propane-oxygen data were obtained from the Distant Plain 2a experiment which utilized a 125 foot diameter hemispherical gas bag containing 20 tons of gas mixture with a theoretical energy yield (based on burning to CO) of 26 tons of TNT. Above 40 psig the propane-oxygen data fall below the nuclear data, while below 7 psig the propane-oxygen data lie above the nuclear data. There is some disagreement between the Ballistic Research Laboratory (BRL) and Canadian data; as will be discussed later some of the data are suspect. The cited references do not present raw data and do not contain details of the circuitry, system response or calibrations, making it difficult to draw firm conclusions regarding the accuracy of the data. The propane-oxygen calculation and data, for the most part, exhibit positive curvature in the pressure, distance plane, in agreement with the nuclear curves.

The details of the hydrodynamic expansion of the explosion products are crucial in determining how closely a chemical explosion replicates the blast effects from a nuclear explosion, especially at ranges where the mass of air engulfed by the blast wave is less than ten times the mass of the chemical explosive. The sound speed, the density, the physical size of the detonation products, and the energy partition all determine the rate of decay of the peak pressure curve. It is not surprising that different chemical explosives produce blast wave decay rates that differ one from the other and that all differ from a nuclear explosion. To further illustrate this fact, the peak pressure vs. distance curve of TNT is compared with nuclear data and a gaseous explosion calculation in Figure 2.2. The TNT curve is based on a 20 ton surface burst scaled from a free-air calculation [8]. The calculation is closely matched by experimental TNT explosion data. The nuclear curve is scaled from the U.S. '59 curve and the methane-oxygen curve is scaled from a calculation performed for the Distant Plain program. Because of the high density and the low temperature of the TNT detonation products, the TNT blast pressure decays more slowly with distance than does the nuclear, exhibiting negative curvature rather than positive curvature above 10 psig. The decay curves follow each other fairly well over a limited range between 2.5 to 15 psig. The

methane-oxygen calculation shows but a small offset from the U.S. '59 curve between 7 and 200 psig. Although propane-oxygen and methane-oxygen detonations have intrinsic differences, e.g. the detonation pressures are different, one of the main reasons for the difference between the goodness of fit to the nuclear curve for simulation purposes is that for the Distaint Plain program the propane overpressure decay curve was fit to match the TNT curve in the range from 10 to 15 psig [9], while for the purpose of the present program the methane curve was scaled to give a best fit to the nuclear data. Because of the offset between the TNT and nuclear curves, and especially because the TNT curve has the wrong curvature above 10 psig the rationale for designing a simulator to match the TNT curve above 10 psig (or at any pressure) is obscure. It is clear that a gaseous explosion produces a better fit to the nuclear overpressure vs. range curve than does a TNT explosion, and by induction a fuel-air explosion should also be superior to a solid detonation.

The goodness of the fit between either the methane-oxygen or the propane-oxygen and the U.S. '59 curve is based on a minimum offset between the curves. The slopes do not match as shown by the propane-oxygen data in Figure 2.3. At high pressure the propane data fall near the 20 ton nuclear surface burst curve while at low pressure the data fall near a 40 ton nuclear surface burst curve. A similar discrepancy is apparent in a comparison of the positive phase impulse for the nuclear and gaseous detonations, Figure 2.4. At high pressure (close-in ranges) the propane-oxygen static impulse lies on a 40 ton nuclear surface burst curve, but at low pressure (far ranges) the propane static impulse exceeds the nuclear.

Ultimately, the quality of a blast simulator must be judged by how closely the simulated static pressure and dynamic pressure waveforms match the nuclear waveform. It is crucial that the simulated impulse match the nuclear impulse within the quarter-period response time of test structures. It is believed that differences in impulse should not exceed 10 to 20 percent of the nuclear impulse within the quarter-period time. As the blast simulator program proceeds, the quarter-period criterion should be refined

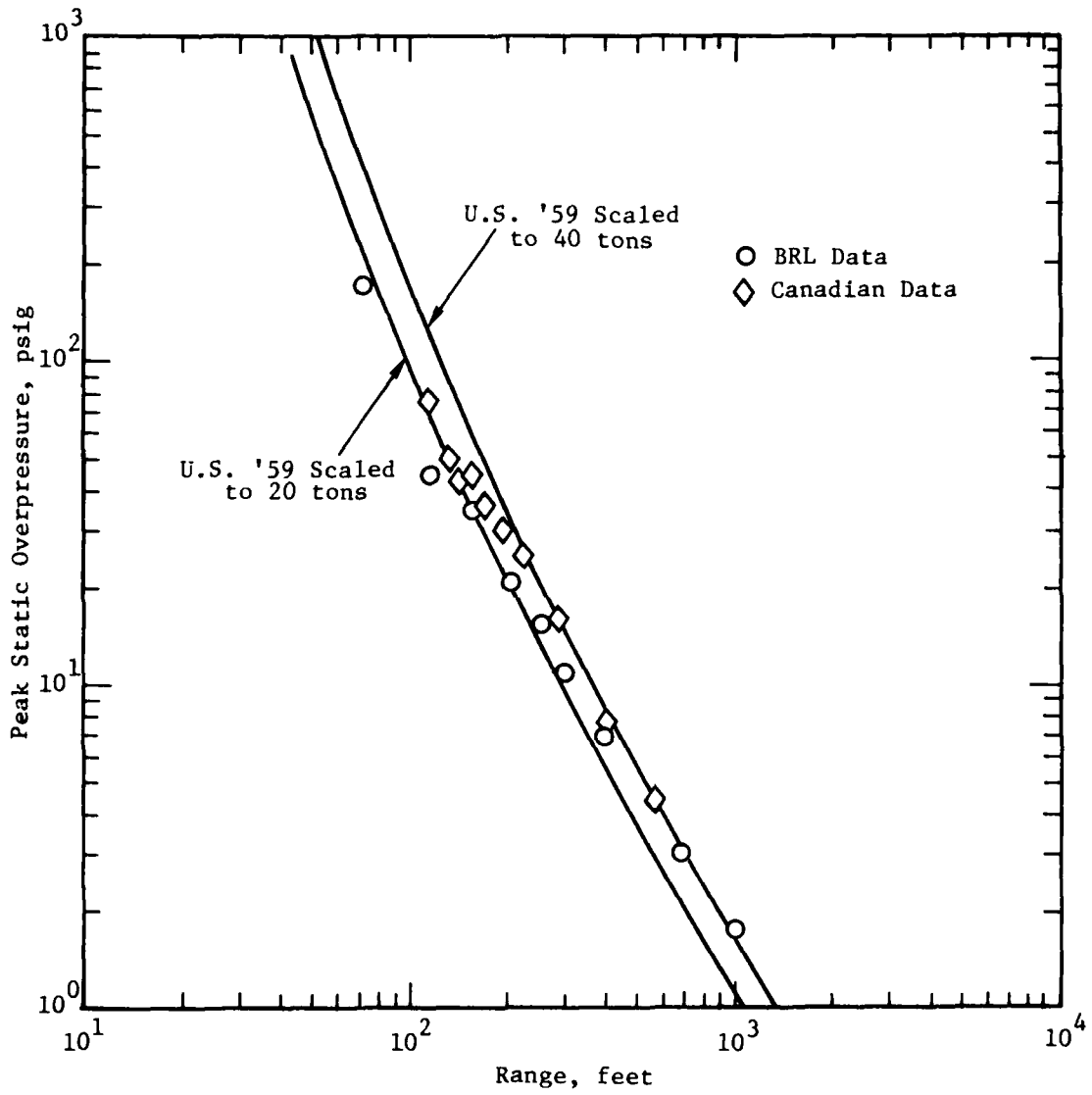


Figure 2.3 Propane-oxygen surface burst peak pressure data compared with nuclear surface burst data scaled to 20 tons and 40 tons.

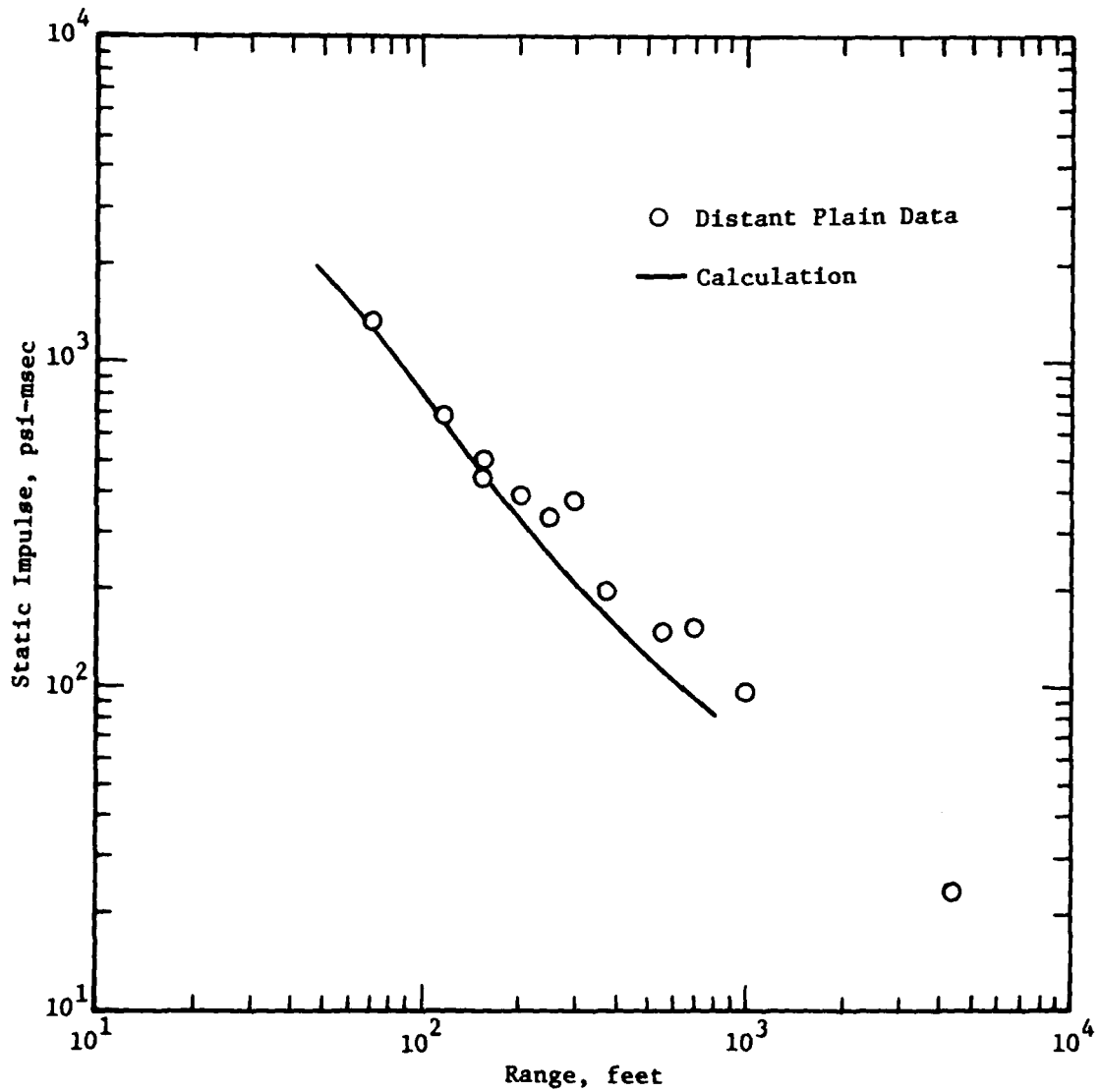


Figure 2.4 Propane-oxygen positive phase static overpressure impulse data compared with a nuclear surface burst calculation scaled to 40 tons (Brode).

and the goodness of fit for times exceeding the quarter-period should be established. Late-time differences must be small enough so that failure under simulated loading does not occur where none would occur under nuclear loading. Because of the offset that exists between the chemical and nuclear driven overpressure vs. range curves the concept of scaled range for a fixed yield lacks utility; hence, the simulated and nuclear waveforms are herein compared on the basis of peak overpressure irrespective of the range. For the purposes of this review the nuclear waveforms are idealized by using the results of machine calculations [10], which provide a fair match to experimental nuclear data. It is important to note that the calculations do not extend below 2 psig and should not be extrapolated below this pressure. Moreover, data from large-yield nuclear explosions suggest that atmospheric effects can cause a substantial departure from the ideal overpressure waveforms below about 3 psig. The data presented in this section were replotted with a precision of approximately 1.5% from data reports. Data copied directly from the source material are presented in Appendix B.

Four comparisons are made between chemical driven blast waveforms and nuclear waveforms. A propane-oxygen overpressure waveform (Distant Plain 2a) with a peak overpressure of 35 psig is compared with a 40-ton nuclear waveform in Figure 2.5. The simulated total positive phase impulse is 32% greater than the nuclear. Within a 10-ms quarter-period response time, which is typically a minimum response time for many above ground hardened structures, the simulated impulse is 20% greater than the nuclear. The simulated waveform is thought to be just barely adequate for structural testing. A TNT driven waveform (Middle Gust II) scaled from 100 to 20 tons with a peak pressure of 24.2 psig is compared with a 20-ton and a 40-ton nuclear waveform in Figure 2.6. The agreement with the 40 ton nuclear case is quite good. Good agreement is also obtained on the same experiment at a peak pressure of 66.4 psig, Figure 2.7. The need for accurate measurements and calculations in the fuel-air program is suggested by the propane-oxygen data in Figure 2.8. At an apparent peak pressure of 21.2 psig the chemical

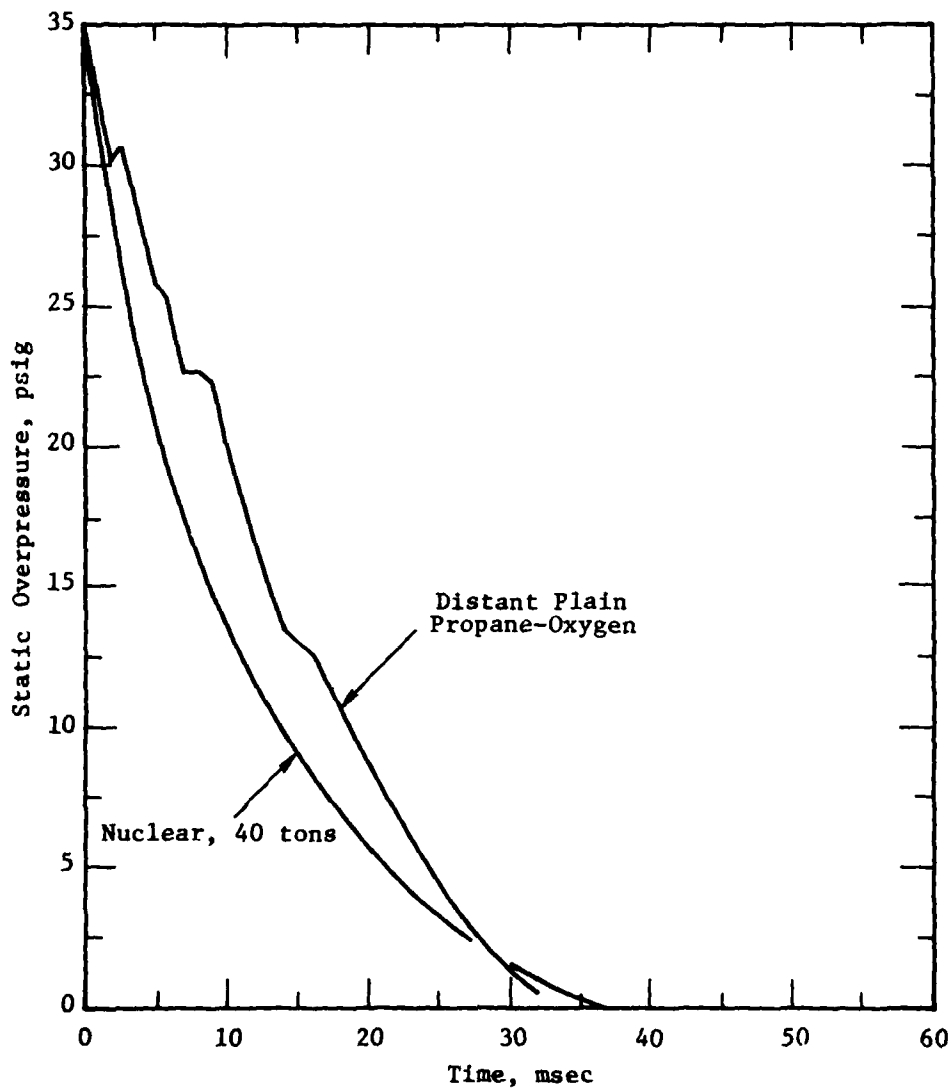


Figure 2.5 Propane-oxygen waveform (BRL) vs. the nuclear waveform (Brode) at 35 psig. Propane-oxygen waveform replotted from Operation Distant Plain surface data at a range of 155 feet (Appendix B).

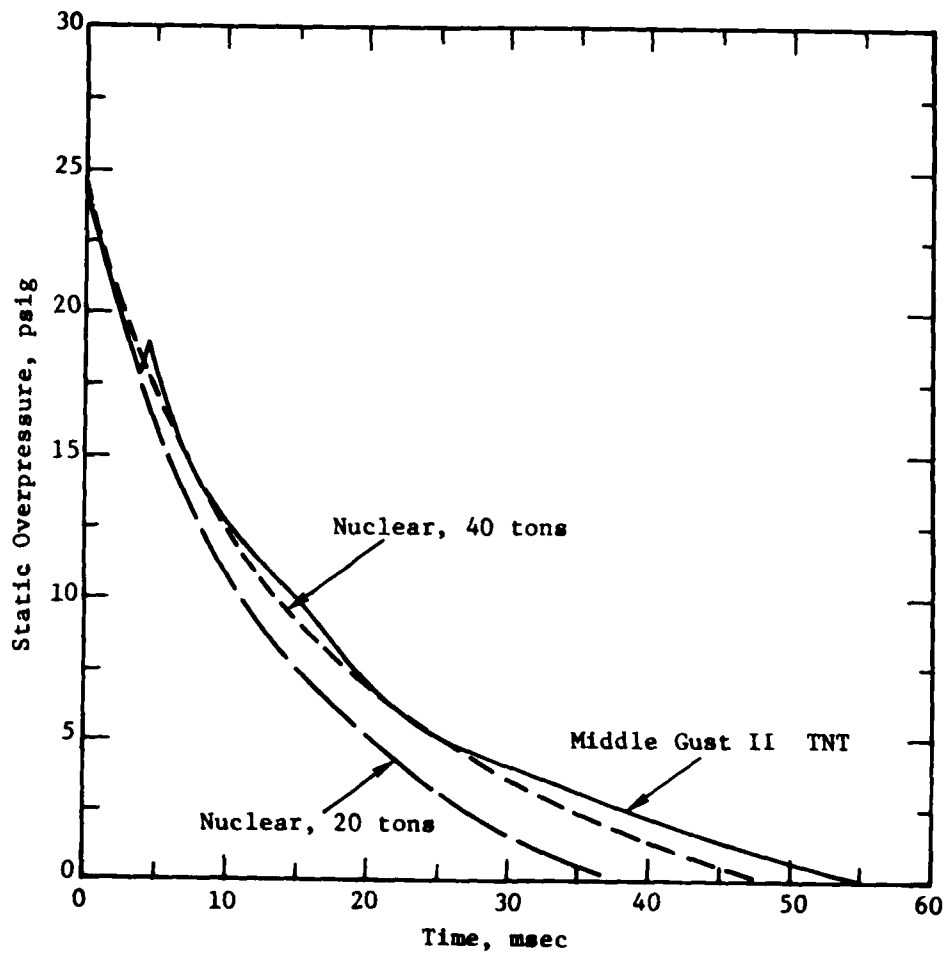


Figure 2.6. TNT overpressure waveform (AFWL) vs. the nuclear waveform (Brode) at 24.2 psig. TNT waveform replotted from Middle Gust II data at a range of 400 feet (Appendix B) and scaled to 20 tons.

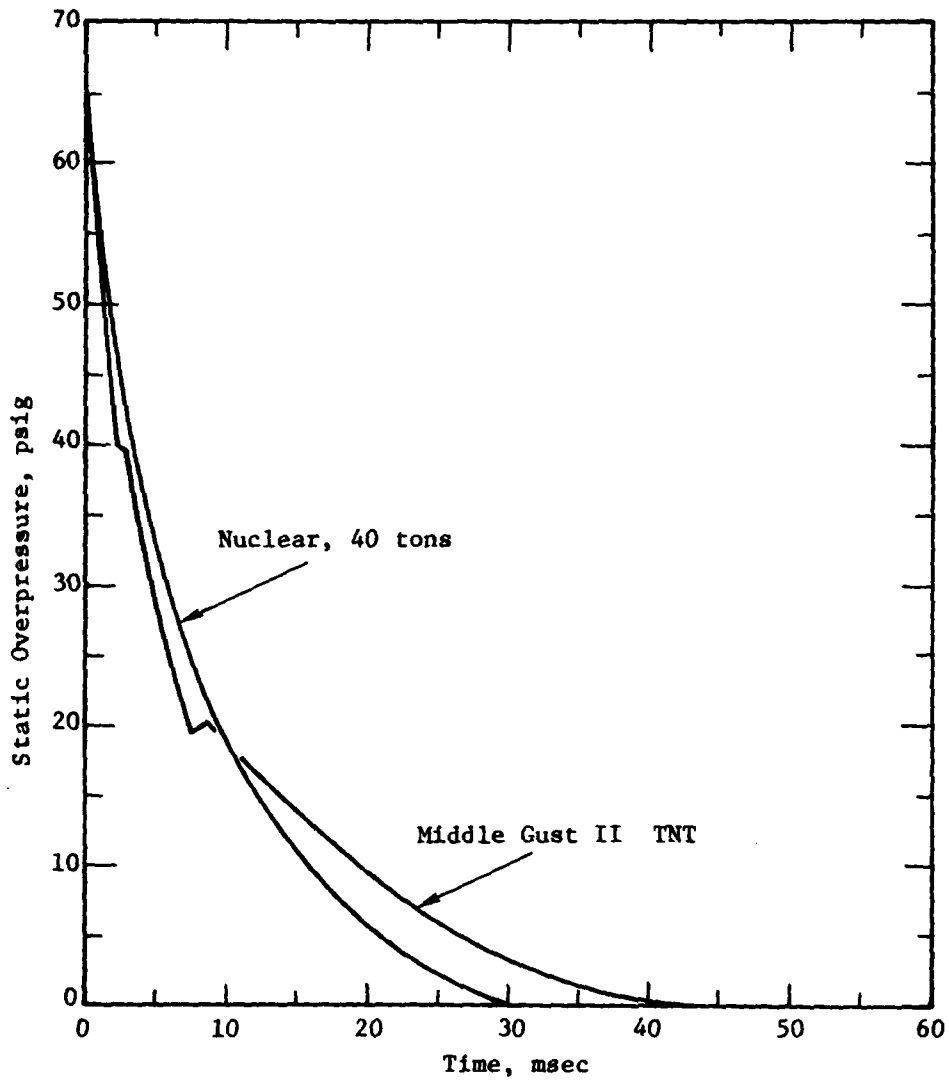


Figure 2.7 TNT overpressure waveform (AFWL) vs. the nuclear waveform (Brode) at 66.4 psig. TNT waveform replotted from Middle Gust II data at a range of 280 feet (Appendix B) and scaled to 20 tons.

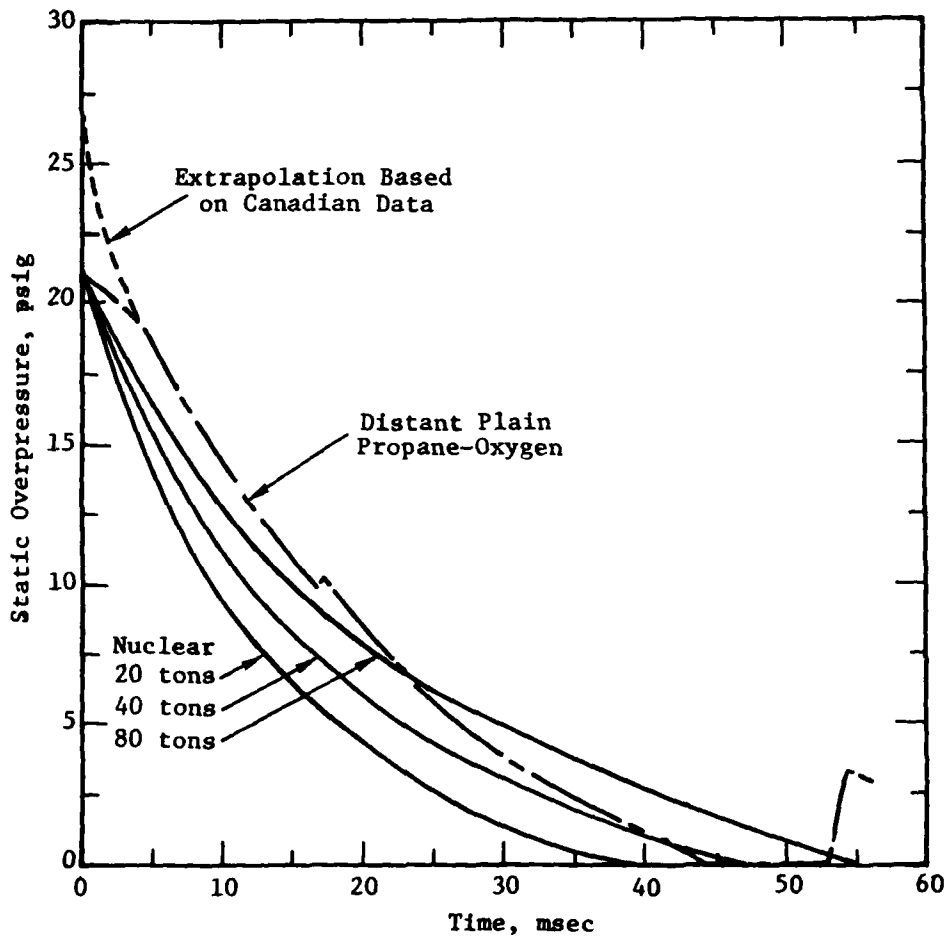


Figure 2.8 Propane-oxygen waveform (BRL) vs. nuclear waveform (Brode). Propane-oxygen replotted from Operation Distant Plain data at a range of 200 feet (Appendix B).

waveform initially exhibits negative curvature in the pressure, time plane and consequently builds impulse at a much faster rate than the nuclear waveform. Neither 20, 40, nor 80 ton nuclear waveforms can match the simulator waveform. Based upon other data [11] it is believed that the peak pressure was in fact 27 psig, not 21.2 psig, which would give a positive waveform curvature in agreement with nuclear data. Negative curvature waveforms may occur in practice as demonstrated by machine calculations of TNT driven waveforms [12]. The negative curvature occurs in shocked air, but within a region that is overrun by explosion products. A series of shock waves within the detonation products also cause further departures from nuclear waveforms. These deleterious effects for TNT driven blast waves can occur at peak pressures as low as 300 psig. Analogous calculations of fuel-air explosions are necessary to ensure that the simulator waveforms are theoretically capable of replicating the nuclear data.

Based on the foregoing comparisons, a fuel-air airblast simulator program must place emphasis on the accurate measurement of waveshapes to allow comparisons to be made with nuclear waveforms. Accurate calculations of fuel-air blast waves would assist in determining whether departures from nuclear waveforms are intrinsic to the chemical detonation, are caused by non-ideal detonation phenomena, or are caused by instrumentation errors. Careful step response gage calibration is required. Additional analyses comparing drag induced loading by fuel-air and by nuclear explosions are also necessary.

SECTION 3

FUEL DISPERSAL AND DETONATION

3.1 FUEL DISPERSAL TECHNIQUES

Before the decision was made to use liquid jets for fuel dispersal three techniques were proposed for the dispersal of liquid fuels; namely, the boil-off of high vapor pressure liquids, explosive dissemination, and high velocity liquid jets. Each of the three techniques may have several variants. The basic ideas are reviewed in Sections 3.2 to 3.4, with liquid jets being discussed in some detail. As a starting point, it is assumed that between 75,000 and 150,000 kg of liquid fuel are required to simulate the blast effects from a 1-KT nuclear device.

3.2 BOIL-OFF

Experiments have been performed at Sandia Laboratories, Albuquerque in which tanks containing up to 450 kg of volatile fuel were opened to the atmosphere [13]. Three schemes were used. Multiple nozzles fed by the static pressure in the tank were used to direct the fuel into the atmosphere. Pressurizing the tank was also tried, but did not enhance the spreading of fuel. This negative result implies that the nozzles were choked and that a larger throat area is required. Cutting off the top of the tanks with an explosive line charge was also tried. All three methods produced detonable fuel-air mixtures, but in all cases the mixing was non-uniform, leading to regions of rich and lean mixture. A practical and economical technique for obtaining a useful height-to-diameter ratio of a cloud produced by boil-off from multiple tanks needs to be derived before the idea can be seriously considered. A set-up of multiple tanks including some tanks elevated off the ground to obtain a useful height-to-diameter ratio could be used to advantage to quickly obtain data on the existence and magnitude of multiple cell effects. A first cut at dispersal rates and height-to-diameter ratios could be obtained by analysis of Sandia motion picture films.

3.3 EXPLOSIVE DISSEMINATION

The advantages of an explosively dispersed fuel system are several. At the outset of a feasibility program the concept allows multiple cell effects to be investigated at minimum fixed cost and at reduced scale. Unlike the boil-off technique, fuels with a low vapor pressure can be used, e.g. gasoline or kerosene. The dispersal is more rapid than the boil-off scheme and should be less affected by winds.

3.4 LIQUID JET PROPAGATION AND DISPERSAL

In this section the problem of dispersing 75,000 kg of liquid fuel into a 160-meter diameter cylindrical volume 53 meters high by means of liquid jets is addressed. These figures are chosen as a starting point to give a fuel-air ratio of approximately 0.06 and a height-to-diameter ratio of 0.3. It is assumed that the liquid has a density $\rho = 700 \text{ kg/m}^3$, a kinematic viscosity $\nu = 5 \times 10^{-5} \text{ m}^2/\text{s}$ and a surface tension $\sigma = 22 \times 10^{-3} \text{ N/m}$.

The simplest arrangement would be to inject the liquid from a planar array of nozzles on the ground at the base of the cylindrical volume of air. Then, with a minimum of 200 jets in the array to ensure uniform dispersal, it will require jets of diameter $D = 2 \text{ cm}$ pressurized to 5,000 psi (nozzle velocity = 300 m/s) for 5 seconds to pump the required 100 m^3 of liquid. The problems with such a design will be pointed out in the discussion that follows.

The required jets would have such a great speed and high Reynolds number that there are no experimental data available in the literature concerning their behavior, especially at large distances from the nozzle. Analytical estimates must be made by extrapolating established empirical relations by orders of magnitude. It would be very unwise to base a final design on such calculations. Model experiments must be performed before establishing any design. In the sections that follow, information relevant to the FAF application available in the existing literature are summarized.

3.4.1 Jet Design

It is well-known that conventional liquid jets operating below the critical temperature are very stable and do not spread very rapidly. Thus,

it is just conceivable that if low volatility fuel jets were sprayed from straight-pipe nozzles, they would extend out to an average distance of 2,600 diameters, as required by the first cut at the FAE design. The Weber number, $We = \rho u^2 D / \sigma$, of these jets is 6×10^7 ; so the destabilizing effect of surface tension should be entirely negligible. Indeed, an extrapolation (by more than one order of magnitude in \sqrt{We}) of the correlation of Phinney [14] for the break-up length of turbulent jets, suggests that the region in which surface-tension-dominated effects would cause spreading of the jet is about $L/D = 8,600$.

The Reynolds number of the jets is $Re \approx 10^7$, so when the fluid emerges from the nozzles, it is turbulent. One possible approach is to treat the liquid jet as a high density turbulent jet submerged in a low-density ambient fluid. In the present case, for hydrocarbon fuels, the density ratio is about 560. Abramovich's model [15] of such jets using eddy-viscosity concepts predicts that for very high density ratios the jet will grow initially at one-half the rate of a constant-density jet (half-angle = 12 degrees). However, on the basis of a theory in which it is hypothesized that turbulent entrainment is controlled by the "elasticity" of turbulence, Townsend [16] asserts that the eddy-viscosity models vastly overestimate the growth rates for both high- and low-density ratio jets. Townsend shows a picture of a water jet expanding at only about a 1-degree half-angle as substantiation of his prediction. Nevertheless, if the material in a liquid jet reaches an asymptotic state far downstream in which the liquid is finely dispersed, then behavior similar to an ordinary constant density jet (and, possibly in accordance with Abramovich's model) would be expected. Indeed, because the concentration of the liquid decreases (by entrainment of air) in the downstream direction, the growth rate might increase toward that of the constant-density case. Calculations of lateral spreading and the decrease of jet velocity with axial distance based on Abramovich's theory are presented below. The theory is heavily dependent upon the use of Prandtl's third hypothesis for the eddy viscosity which assumes that the eddy viscosity is constant at any fixed cross section of the jet and is proportional both to the jet diameter and

the velocity difference between the centerline and the edge of the jet. In addition, a density weighted velocity correction to account for two-phase flow and self-similar velocity and concentration profiles are employed. The key parameter in the calculated results is the ratio of the density of liquid ρ_l , to the density of air ρ_a . In assessing the validity of Abramovich's theory against experiment, some caution must be exercised because the experiments are for the most part concerned with jet breakup or intermittency effects while Abramovich's theory describes a continuous process in which air is entrained and mixed with a fluid to produce a gradual spreading of a homogeneous two-phase mixture. The work of Phinney [17], which indicates that ρ_a is not important in controlling breakup, suggests that ρ_l/ρ_a may not be, in fact, an important parameter. The validity of Abramovich's theory has not been demonstrated, but at present it is the best that is available.

To continue, the theory indicates that for a liquid jet in the steady state the velocity on the jet axis, u_m , is related to the jet radius, r , and the ratio of the density of liquid to the density of air:

$$\bar{u}_m = 2.25 \frac{\rho_l/\rho_a}{\bar{r}^2} \left[\sqrt{1 + \frac{1.5 \bar{r}^2}{\rho_l/\rho_a}} - 1 \right],$$

where

$$\bar{u}_m = u_m/u_0$$

$$\bar{r} = r/r_0,$$

and u_0 is the jet velocity at the nozzle, while r_0 is the initial radius of the jet.

The jet radius is related to the axial distance from the nozzle by

$$0.22(\bar{x} - \bar{x}_0) = \bar{r} + \sqrt{\frac{\rho_l}{\rho_a}} \left\{ \ln \left(1.22 \bar{r} \sqrt{\frac{\rho_a}{\rho_l}} + \sqrt{1 + 1.48 \bar{r}^2 \frac{\rho_a}{\rho_l}} \right) - 0.25 \tan^{-1} \left(1.28 \bar{r} \sqrt{\frac{\rho_a}{\rho_l}} \frac{\sqrt{1 + 1.48 \bar{r}^2 \frac{\rho_a}{\rho_l}} - 0.24}{\sqrt{1 + 1.48 \bar{r}^2 \frac{\rho_a}{\rho_l}} + 0.31 \bar{r}^2 \frac{\rho_a}{\rho_l}} \right) \right\}$$

where the following auxiliary relations must be used:

$$\bar{x}_n - \bar{x}_0 = 13.6 \sqrt{\rho_l / \rho_a}$$

$$\bar{x}_n = 10.7 \left(1.73 \sqrt{\rho_l / \rho_a} - 1 \right) .$$

In the theory of jets, x_0 is the apparent point source location of the jet, x_n is the location of a transition section which lies somewhat downstream of the point of boundary layer closure, and \bar{x} denotes a normalization with respect to the initial radius of the jet.

The mass concentration of liquid on the axis of the jet in terms of the jet speed is given by

$$\chi_m = \frac{\bar{u}_m}{1.343 - 0.806 \bar{u}_m} .$$

Based on the calculated results, Figure 3.1, not much difference is seen between the lateral spreading and axial slow-down of a water jet ($\rho = 1.0$) and a hydrocarbon fuel jet ($\rho = 0.7$). The mass concentration of liquid on the axis (for a non-volatile fuel) does not fall to a value characteristic of a detonable gaseous mixture until the jet has propagated about

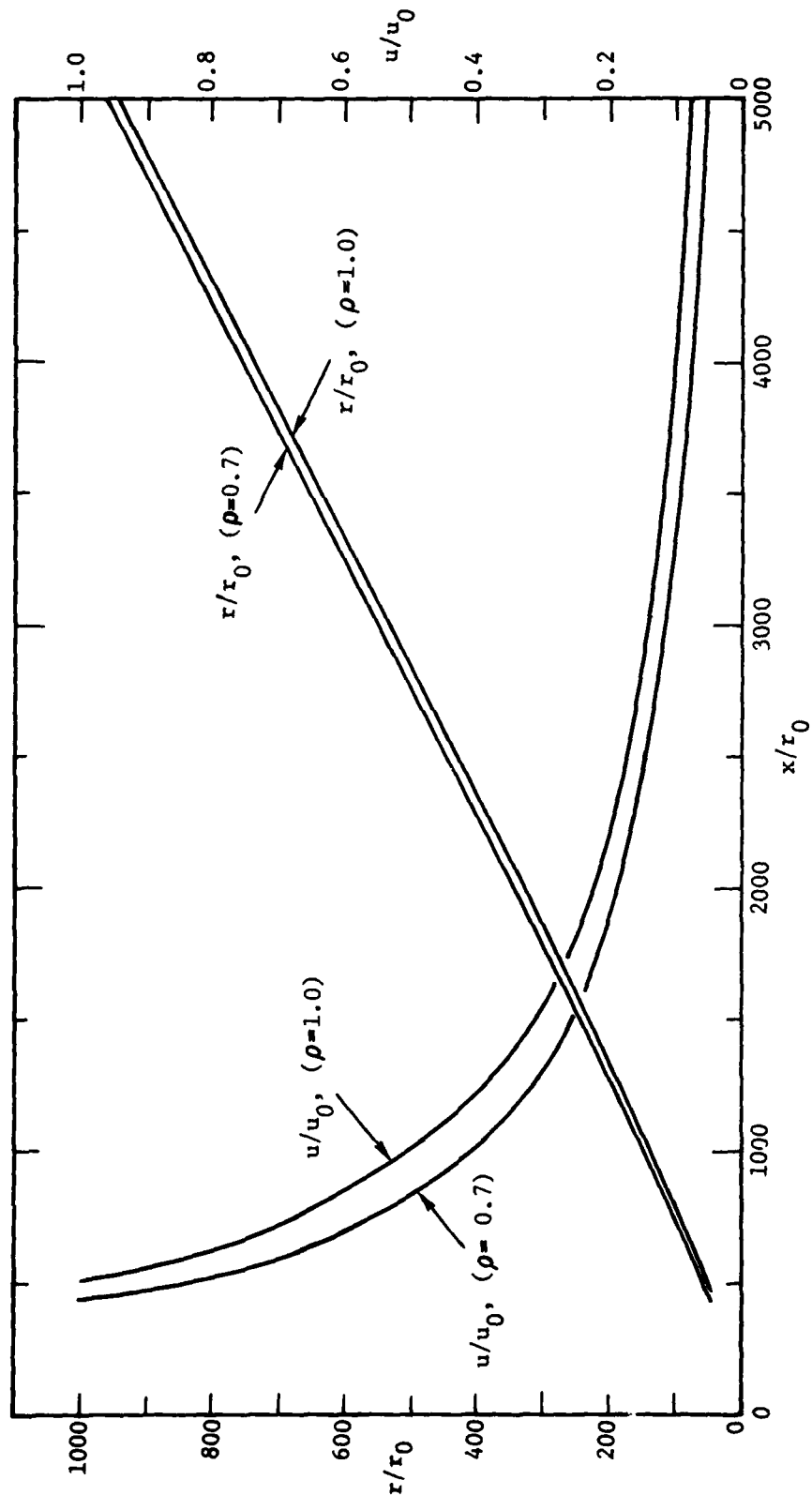


Figure 3.1 Calculated propagation of turbulent liquid jets in air. Jet radius and speed versus jet length.

1000 diameters, Figure 3.2. This result has significant implications for the FAE design and should be tested in the early phases of the experimental program. Although the analysis does not consider the effects of fuel vaporization, it is almost certain that fuel volatility is an important parameter and will modify the results quoted above.

Returning to the initial design problem, Figure 3.1 implies that the jet half-angle is about 10.9 degrees after the jet has propagated 2,500 diameters. Thus, to an order of magnitude, one expects the jet diameter to be about 1000 times the initial diameter, i.e. 20 meters at $L/D = 2,600$. Since there are 200 jets, the average jet spacing is 11 meters, so dispersal near the top of the cylinder should be fairly uniform. The jet centerline velocity at $L/D = 2,600$ is about 6.4% of the nozzle exit velocity or 19 m/s. At the desired height of 53 meters the action of gravity is equivalent to less than 2 m/s of jet velocity, so that fluid will be carried above the desired volume.

The volume dispersion of fuel will almost surely be heavily dependent on droplet mechanics, that is to say, upon the size and number of nascent drops and their evolution prior to detonation. The motion of drops will be affected by natural winds and by the motion of air induced by jet entrainment. The effect of gravity must also be assessed in relation to aerodynamic drag effects. For volatile fuels the effects of vaporization must be known. Based upon FAE weapons work, it appears that little is known about droplet formation. Based upon experience both with particulate flow and two-phase flow experiments it is very difficult to measure droplet sizes in a single stream [18, 19], and it is recommended that such measurements not be attempted. Even if droplet sizes were measured, detonability could not be predicted from first principles, although such data would be useful for comparative purposes. The cost of drop size measurements would exceed that of the entire FAE feasibility program as currently envisioned. The question of drop size should be deferred and emphasis placed on detonability.

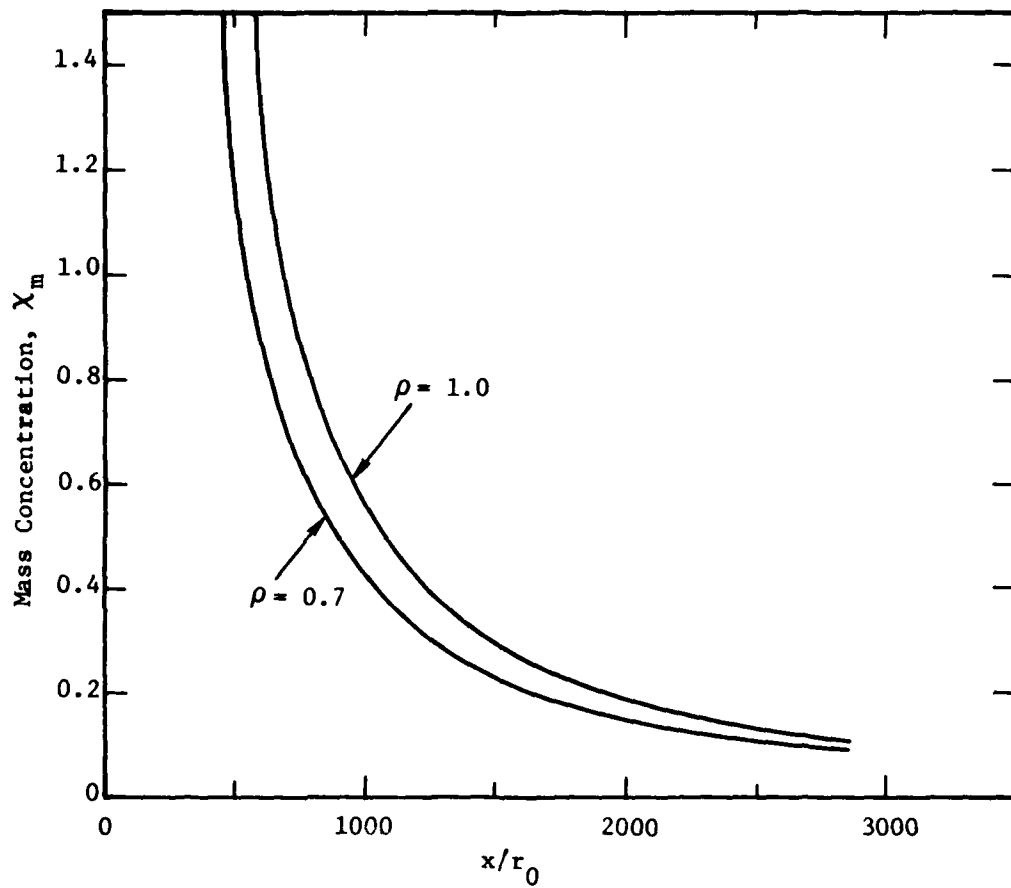


Figure 3.2 Calculated liquid phase mass concentration, X_m , on the axis of a turbulent jet propagating in air versus distance from a nozzle of radius r_0 .

For purposes of an initial design, it is also of interest to consider the behavior of a highly volatile jet operating above the boiling temperature, for example, a jet of propane. Because of the boiling action with the attendant reduction in the average density of the jet, it is likely that the jet half-angle will approach that of a constant density jet (12 degrees). Whether a boiling jet could reach 2,600 diameters is uncertain (and perhaps unlikely). Photographs taken by Benedick [20] of the region around the outflow of a straight glass pipe show that a propane jet immediately expands upon issuing from the pipe. Moreover, a boiling region works its way back into the supply pipe. The design of a two-phase supply system would have to rely heavily on experiments.

It must be emphasized that it would be remarkable if the results of the calculations in this section were correct to within an order of magnitude. However, taken at face value, they indicate that liquid fuel may be dispersed into a large volume of air using rather simple configurations of liquid jets.

3.4.2 Detonability and Types of Fuels

The detonability of liquid fuels is influenced by a variety of factors including vapor pressure, drop size, molecular structure, and free radical formation. Detonability can often be improved by adding a sensitizer or promoter to the fuel. The type of sensitizer needs to be determined. For the purpose of the initial design of FAE, it is noted that a wide variety of fuels have been detonated, including unsensitized kerosene and methane. The relatively costly fuels used in FAE weapons, e.g., propylene oxide, were chosen in part because of their high density relative to air which causes the explosive cloud to hug the ground. No such requirement is imposed on the FAE simulator fuel.

At the outset of the program, detonability is the most crucial item in the entire design. At the present state-of-the-art detonability cannot be determined from first principles, but data on drop size and fuel weight in the vapor phase for a given fuel might allow by analogy with FAE weapons an assessment of whether or not a particular design has a good

chance of detonating. Because the determination of drop size and fuel vapor weight is a major undertaking, it is recommended that the direct approach of attempting to detonate specific dispersal designs be undertaken.

The detonability of a single stream is estimated using both Abramovich's theory to calculate the mass concentration of fuel and experimental data on the detonation of fuel-air mixtures. The concentration profile (which is theoretically self-similar)

$$\frac{\chi}{\chi_m} = 1 - \left(\frac{y}{r}\right)^{1.5}$$

is plotted in terms of χ versus the distance from the jet axis with the jet length-to-diameter ratio as a parameter, Figure 3.3. The lower detonation limit is fairly firm but the upper limit tends to increase with the complexity of the molecular bond. For the case at hand, the jet must be designed to propagate of the order of 1000 diameters to ensure detonation. However, for the design utilizing 200 jets the fuel-air ratio is very non-uniform at $L/D = 1000$, even though essentially all of the liquid fuel lies within the gaseous detonation limits. At the top of the cylindrical cloud, at $L/D = 2600$, the action of multiple jets creates a fairly uniform fuel concentration which lies just above the lower detonation limit for a gaseous fuel, Figure 3.3. The near-conical geometry of a jet causes a cylindrical cloud to have a nonuniform fuel-air ratio. A spherical cloud formed from a central spray head would have a more uniform fuel-air ratio that varied principally with distance from the spray head. Some variation in fuel-air ratio with polar angle would occur because of the increase in jet angle with propagation distance, Figure 3.1. Spherical dissemination is, in fact, the method being investigated for the FAE by Systems, Science and Software (Section 4).

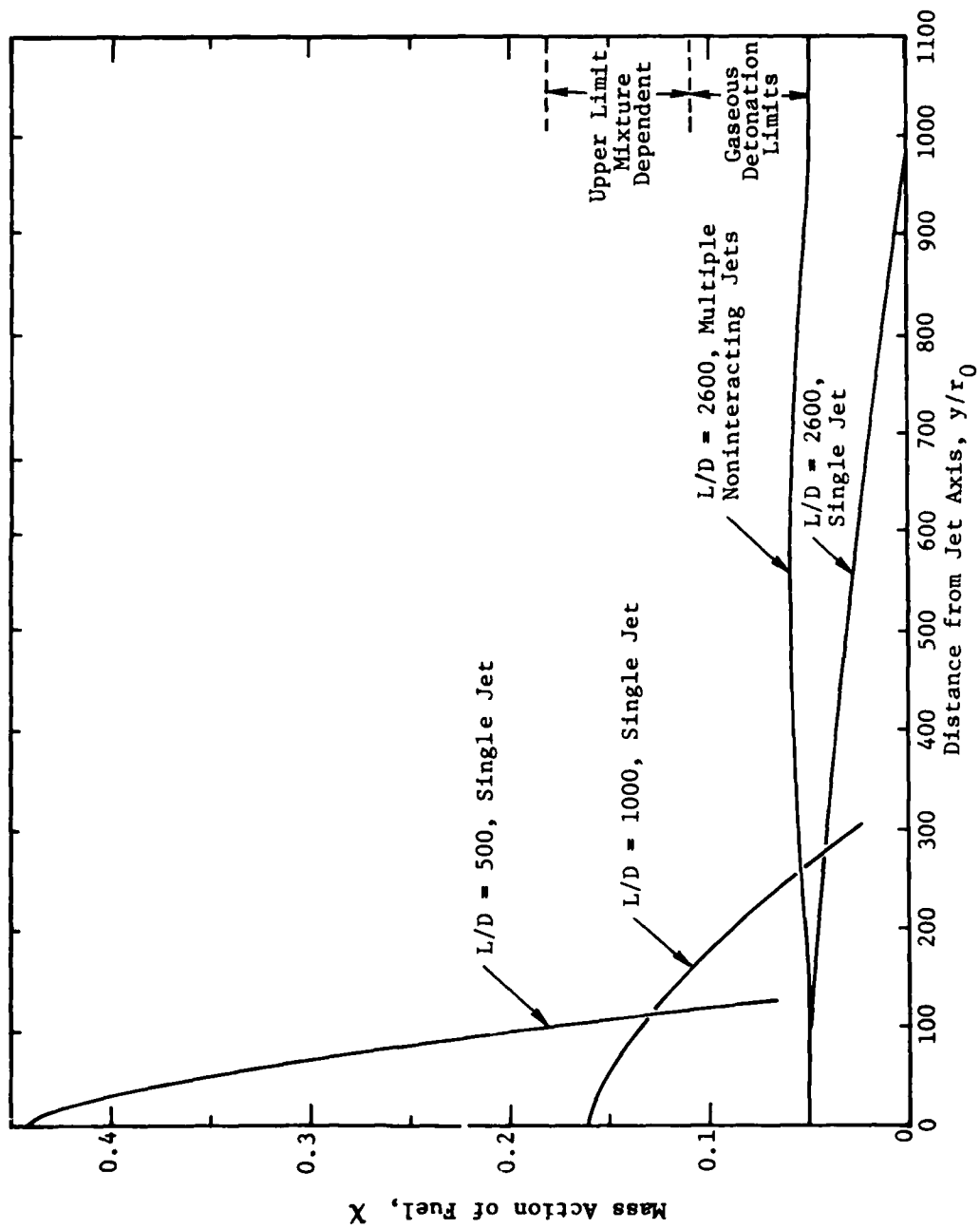


Figure 3.3 Fuel mass concentrations in jets. The multiple jet fuel concentration is based on noninteracting jets spaced at intervals of $y/r_0 = 1100$.

3.4.3 Experimental Data

Experimental data are of two kinds: One type is concerned with jet instability and intermittency effects, while the other is concerned with the effectiveness of water or fire hose streams. The jet instability data have been correlated by Phinney [21] on the basis of the square root of the Weber number such that the length-to-diameter ratio of a stream that breaks up less than 50 percent of the time is given by

$$\frac{L}{D} = 55 + 1.085 \sqrt{We} .$$

Data on intermittency effects are not directly applicable to the problem of the volume dispersion of fuel.

Fire stream data [22] are plotted in the literature in a form that is quite naturally useful to firemen; the data have been replotted in terms of L/D and \sqrt{We} to try to make some hydrodynamical sense out of the data, Figure 3.4. (To eliminate gravity effects to first order, the length of the stream is considered to be the horizontal propagation distance.) The 1-1/2 inch and 2-inch diameter fire stream data do not correlate on the basis of \sqrt{We} . It is noted, however, that for the purpose of making rough estimates of jet reach, Phinney's relation describes the water stream data to within $\pm 20\%$. Defining a length of stream that is significant both for fuel dispersion and for hydrodynamical purposes and at the same time finding valid scaling laws will almost assuredly be a difficult task. At the present time extending extant data to other stream diameters cannot be done in a rational manner. Note that a 2-inch diameter stream does not propagate as many diameters as a 1-1/2 inch diameter stream. It appears that full-scale jets will have to be tested.

3.5 WIND EFFECTS

Depending upon dispersal times a wind cannot only shift the effective center of detonation for an unconfined system but may also adversely affect the dispersal system, e.g., controlling jet interaction may be

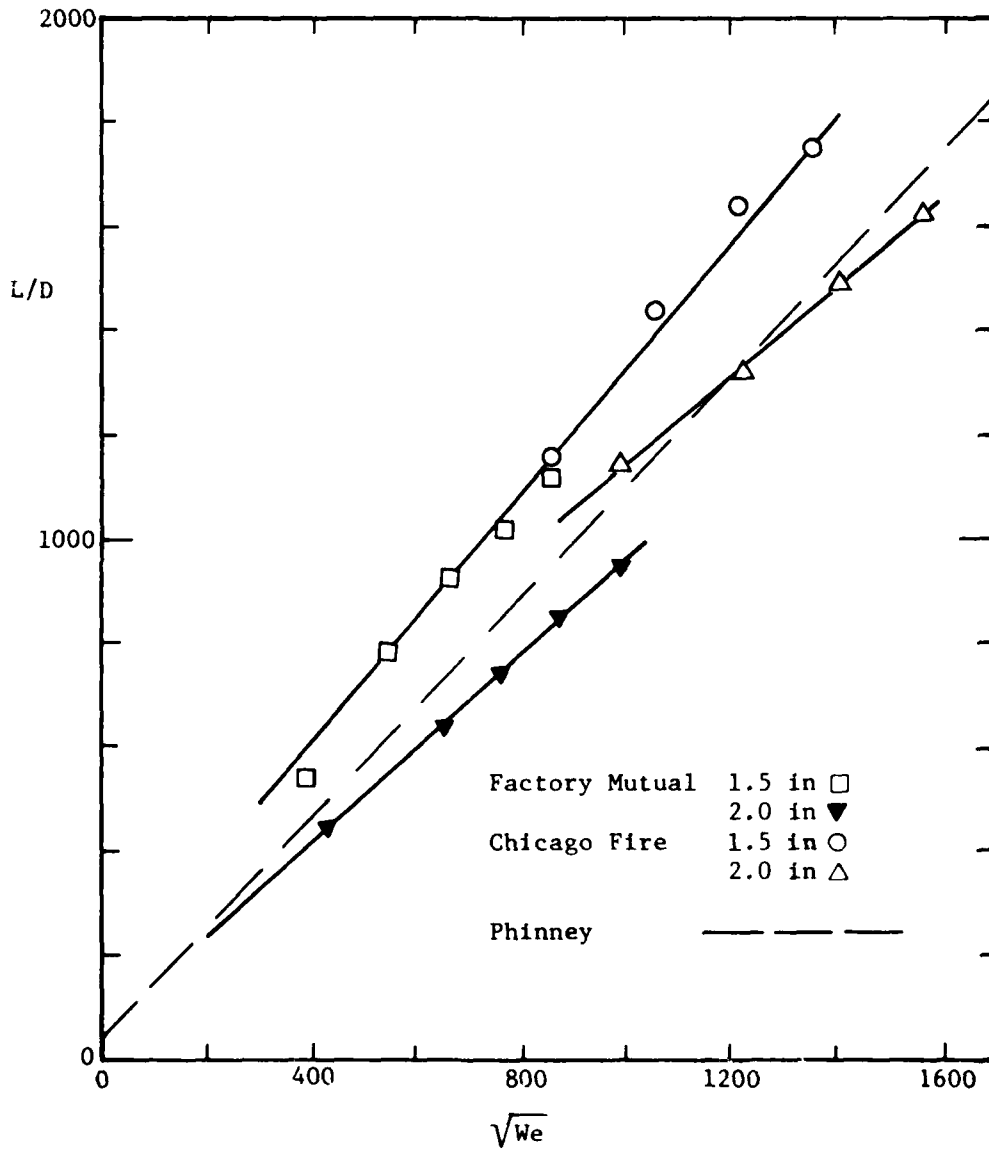


Figure 3.4 Water jet (fire stream) data plotted as L/D versus \sqrt{We} . Although the 1-1/2 and 2-inch data remain distinct in the L/D - \sqrt{We} plane, the relation used to describe jet disintegration $L/D = 55 + 1.085 \sqrt{We}$, fits the fire stream reach to within $\pm 20\%$.

difficult, and a jet system might work only in a quiescent atmosphere. For certain types of unconfined systems, the effective center might be forced to occur at the geometric center of the test array by varying the dispersal sites as the wind velocity varies. Such a system would not be overly complicated but would require additional hardware. Because the control of wind effects on an unconfined system will impose some additional costs on the system, the use of confinement should not be rejected at the outset. For equal costs, an unconfined system is preferred because of the possibility of plastic debris (the confinement) interfering with pressure measurements.

3.6 TEST PROGRAM AND INSTRUMENTATION

The three fuel dispersal concepts are sufficiently uncertain in their operation that small-to-moderate scale tests are required. The initial tests should not be elaborate and could be accomplished both expeditiously and economically. It is crucial to use a sufficient number of accurate, well calibrated airblast overpressure gages. The gage data can be used to infer energy conversion efficiencies, the existence of asymmetries, reproducibility, and the goodness of fit to nuclear data. Based on experience with other liquid fuel detonability programs, accurate field-grade fuel concentration instrumentation is not currently available. The same is true for droplet size instrumentation. Attempts to use extant instrumentation to make either concentration or droplet size measurements inside the fuel cloud prior to detonation will almost surely lead to naught. Attempts to develop new instrumentation will either delay or add unnecessary costs to the program. The FAX concept is in a rather elementary state and much progress could be made in a short time by some rather straightforward experiments.

SECTION 4

THE EXPERIMENTAL PROGRAM

In Section 4.1, guidelines on conducting an experimental program, which were drawn up to assist the FAE feasibility program, are set forth. In Section 4.2, the results of some small-scale FAE experiments performed by Systems, Science and Software are reviewed.

4.1 PROGRAM GUIDELINES

Extant theory and experimental data should be used to estimate jet reach, lateral spreading and fuel concentrations to aid the design of experiments. When examining experimental data underlying scaling laws should be sought.

The main emphasis in the program should be on a series of rational experiments rather than, say, machine calculations. Table 4.1 lists the important unknowns that must be quantified as a function of the indicated parameters.

The main experimental diagnostics will be motion picture photography and blast pressure measurements. There is considerable room for skillful photographic diagnostics. For the initial experiments, a high pressure air driver will prove more versatile and allow faster turn-around time than a chemical propellant. The determinations of detonability, spray characteristics, and similarity to nuclear explosions are the most important aspects of the initial phase of the feasibility program.

4.2 REVIEW OF EXPERIMENTAL FAE DETONATION AND JET PROPAGATION DATA

Small-scale experiments employing a central spray head dispensing 50 lbm of propylene oxide, C_3H_6O , into a 15-foot radius hemispherical volume were used to study the feasibility of the FAE concept. Details of the experiments conducted by Science, Systems and Software, are described in Reference 23. The experiments demonstrated that it is possible (and at least in the small, practical) to use liquid fuel jets to create a detonable hemispherical mixture. The similarity between the low pressure blast effects produced by the fuel-air detonation and a nuclear explosion remains to be determined.

Table 4.1 Program guidelines. Unknowns and parameters in the experimental program.

Unknowns	Parameters
1. Jet Reach	Nondimensional groups, nozzle geometry, unsteady flow behavior (including variable driving pressure), wind effects, fuel volatility
2. Breakup, Drop Formation, Volume Dispersion	As indicated above plus multiple jet effects
3. Detonability	Results of 1 and 2 plus chemical composition of fuel, fuel mixtures and sensitizers
4. Collective Effects	Multiple jet behavior

The data are analyzed on the basis of positive phase impulse, a method dictated by the manner in which the measurements were made. Gage calibrations are not available making difficult the task of determining if waveform irregularities have their origin in the detonation process or in the response characteristics of the transducers. The pressure peaks are particularly suspect. Either the gages are unsatisfactory or the detonation is far from being uniform. The integral approach taken in this section will result, at best, in a smoothing over of some of the uncertainties in the data. The waveforms themselves are not compared with nuclear waveforms. Additional experiments which employ accurately calibrated gages with flat response characteristics must be carried out as the feasibility program continues.

The 50 lbm experiments are scaled to a 1-KT nuclear surface burst using a graphical technique in which the 50-lbm data are slid along a 45-degree line in the log impulse, log range plane until a best fit is effected between the fuel-air data and the nuclear curve. A minimum offset

between the fuel-air data and the nuclear impulse curve is achieved with a geometrical scale factor of 16:1 or a yield ratio of 4100:1. At high static overpressures (approximately 100 psig) the static impulse scaled from the fuel-air explosion falls below that generated by a nuclear explosion, but at low pressure (approximately 10 psig) the opposite is true, Figure 4.1. Thus based on the impulse produced by 50 lbm experiments 205,000 lbm of propylene oxide appears to be required to simulate the airblast effects between 1 and 100 psig from a 1-KT surface burst. The energy released by the 205,000 lbm of propylene oxide can be compared to a 1-KT nuclear explosion in the following way. By using the following simple model,



an upper bound on the specific energy released at constant volume by propylene oxide is estimated to be

$$Q = \frac{10^3}{58} (3 \times 94.052 + 3 \times 57.798 - 0.592) \text{ calories/gram of fuel.}$$

$$= 7884 \text{ calories/gram of fuel.}$$

The enthalpy of formation of CO_2 contributes 94.052 kilocalories per mole, H_2O contributes 57.798 kilocalories per mole, and the conversion from a constant pressure to constant volume process subtracts 0.592 kilocalories per mole. Neglecting the enthalpy of formation of C_3H_6O is estimated to result in an error of approximately 5%. Thus 205,000 lbm of propylene oxide releases a maximum of 7.3×10^{11} calories or approximately three-quarters of one kiloton of energy. These figures must be used with caution until better waveform measurements are available. If the impulse is built-up at relatively late times, then the comparison between the fuel-air and nuclear explosion can be misleading and the energy release is not as efficient in creating blast as might first appear. As discussed in Section 2 comparisons must also be made on the basis of waveforms.

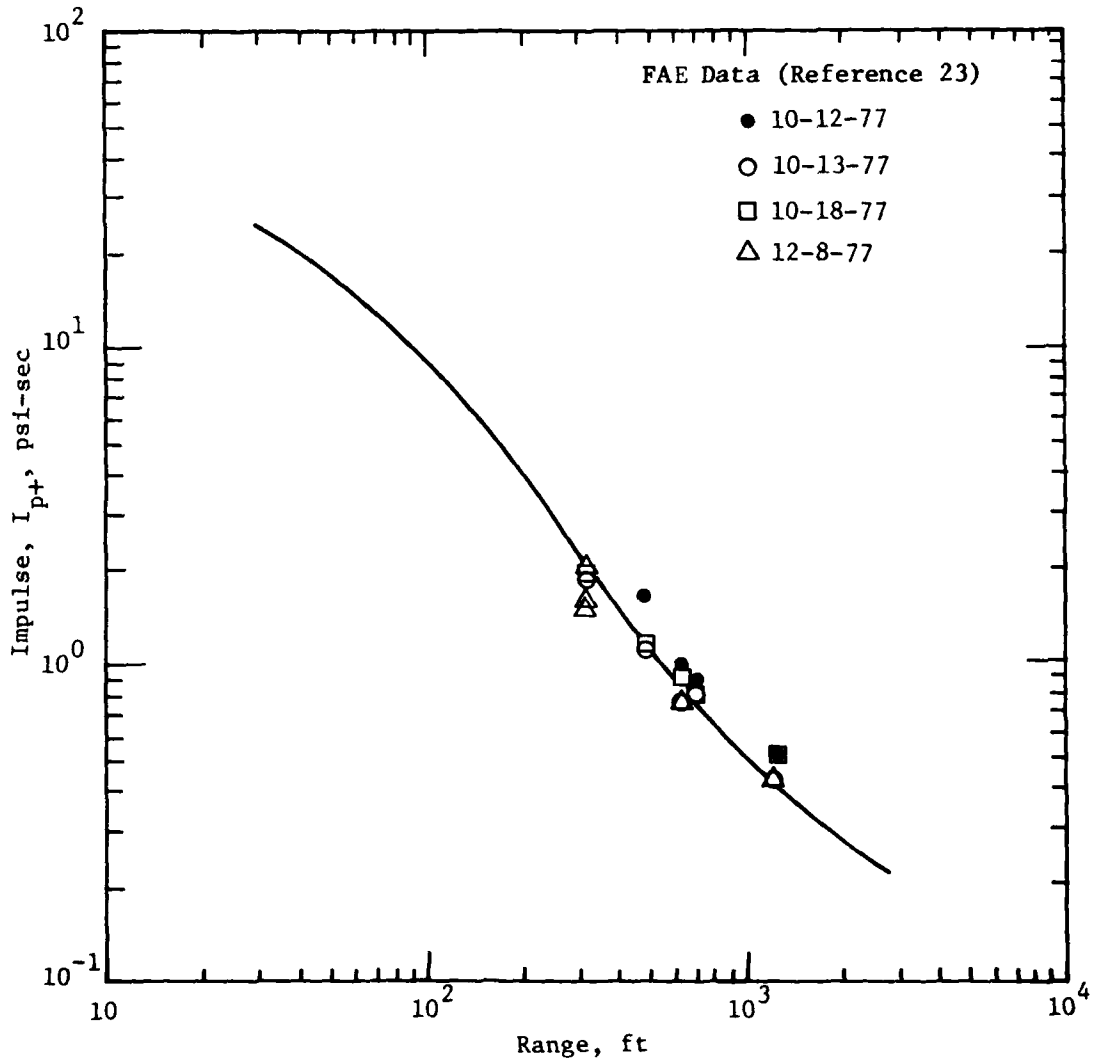


Figure 4.1 FAE positive phase overpressure impulse data (S^3) scaled to fit a 1-KT nuclear surface burst (Brode).

The peak static overpressure data produced by the scaled FAE generally fall below the U.S. '59 surface burst curve, Figure 4.2. Detailed analyses of the peak pressure curve must be deferred until better data are available. Figure 4.2 does illustrate, however, an important aspect of the simulation of nuclear effects which is worthy of discussion. The scatter in the nuclear data upon which the U.S. '59 curve is based are noted by upper and lower bound curves below 10 psig. The upper bound peak pressure curve is about 20 percent greater than the mean, while the lower bound curve is approximately 30 percent less than the mean. (The scatter bounds above 10 psig are not plotted because the necessary data are not readily available.) A variety of causes can be responsible for the scatter including terrain effects, atmospheric effects, transducer response, gage positioning errors and data reduction techniques. It is unlikely that uncertainties in the data will ever be fully resolved because of test limitations; hence, it is prudent to consider the bounding curves when establishing damage criteria. The wisdom of using bounding curves has been demonstrated on underground nuclear tests.

The jet reach experiments reported in Reference 23 were preliminary in nature and cannot be interpreted to provide definitive answers. Nonetheless, they suggest the existence of problems in scaling up the 15-foot FAE design. Qualitative data on transient jet reach vs. jet geometry and stagnation pressure, Table 4.2, indicate that for a volatile fuel (propylene oxide) the ultimate L/D decreases as the initial jet diameter increases, but that the decrease is sufficiently slow that the reach increases with increasing diameter. A similar behavior was reported for steady water jets (Section 3.4.2). The interpretation of the jet reach experiments is beclouded because the jets were not geometrically scaled-up in a way that would be useful for a full-scale test; instead the mass of fuel was set at 50 lbm. A scaled-up jet would contain at least 340 lbm of fuel. The jet reach required for a full scale facility depends upon the mass of fuel needed and the average fuel-air ratio. If it is assumed, for

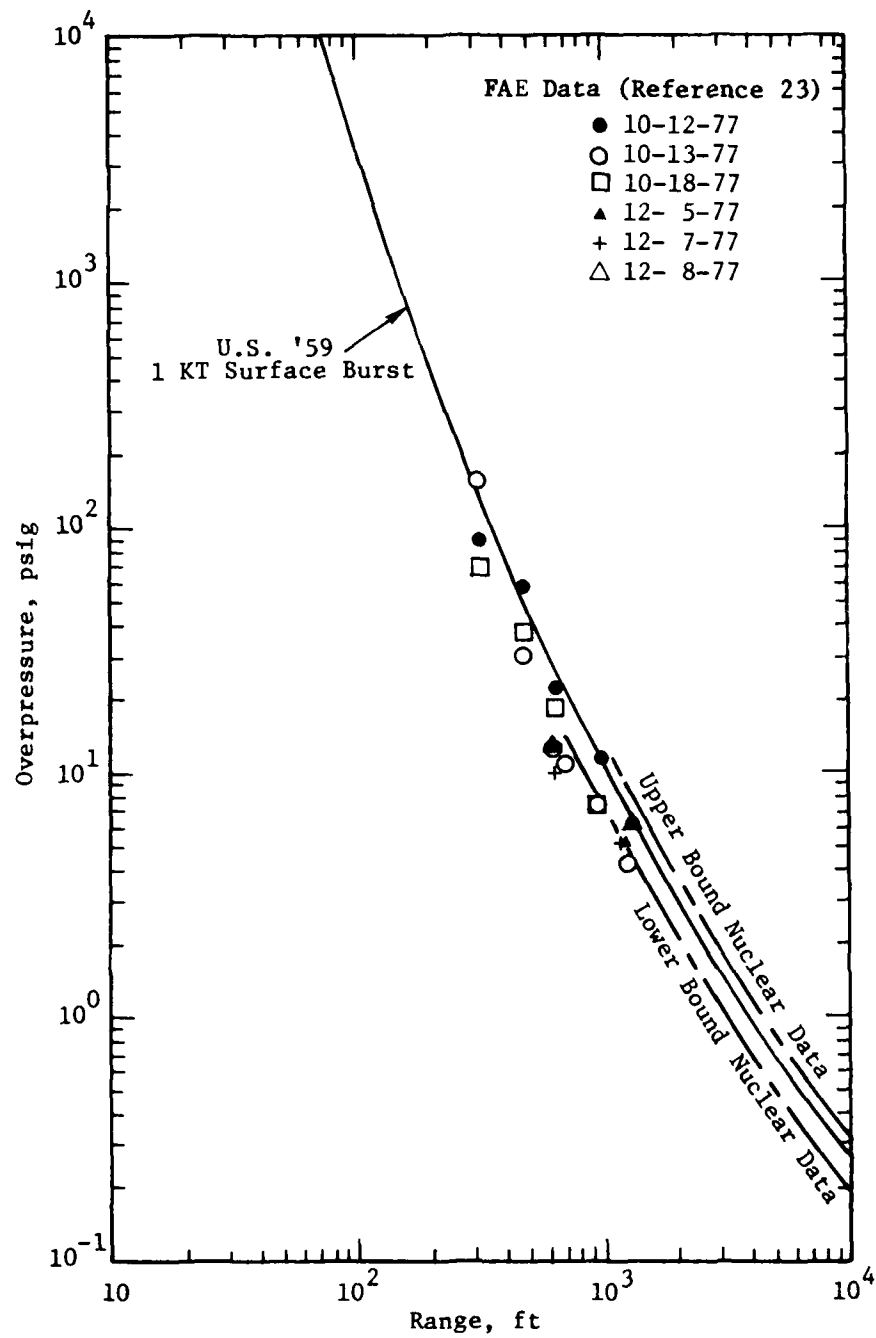


Figure 4.2. FAE peak overpressure data (S^3) scaled to 1 KT surface burst and compared with the U.S. '59 curve.

Table 4.2 Propylene oxide transient jet performance (Reference 23)

Nozzle Diameter inches	L/D	Exit Velocity m/s	Pressure psig
0.125	1440	40	~100
1.5	1290	45	120
2.5	900	72	320

the moment, that the mass of fuel is invariant with fuel-air ratio then using 205,000 lbm of propylene oxide as previously calculated results in a jet length that lies between 235 and 299 feet as the fuel-air ratio varies between 0.1055 (stoichiometric) and 0.05 (the lower detonation limit). So far all experiments have been based on the 15-foot hemispherical tests which have a fuel-air ratio of 0.0987 (based on a jet length of exactly 15 feet and a temperature of 20 degrees C). The effects of varying the fuel-air ratio need to be examined.

Taken at face value the results indicate a lack of geometrical similitude and suggest that the fuel-air ratio produced by jets of different diameter is not invariant at scaled lengths along the jet. It follows directly that the behavior of a full-scale FAE need not be similar to that of the 15-foot FAE. This tentative conclusion is sufficiently important to warrant a careful review of jet experiments during the next phase of the feasibility program. At the present time the test program can go in two directions, but common to both is the requirement to produce long range jets with a length of between 235 and 299 feet. Because of the difficulty in determining drop size and fuel-air ratio (Section 3.4.1) and then relating these quantities to detonability and energy release the direct approach of attempting to detonate single jets has been followed. This approach runs into operational difficulties because a single full-scale jet has a theoretical energy release of 3300 lb nuclear which exceeds the explosive limit of most test sites. Thus, the FAE program can either test full-scale jets

at, say, the Nevada Test Site (NTS) or test a series of intermediate-scale jets. A cost-benefit analysis is needed to make a sound decision, but based simply on experience the cost of testing at NTS is sufficiently high and the extant knowledge about transient long reach jets is so limited that a series of sub-scale tests is a proper course of action. A set of single jet experiments for testing scalability and at the same time providing a basis for designing blast sources with a useful yield are listed in Table 4.3. Except for the full-scale jet the fuel weight has been limited to less than 50 lbm so as not to exceed the explosive weight limit of the Green Farm Test Site. The tests are based on simple geometrical scaling of the 15-foot hemispherical FAE tests, which at the current state of understanding of jet performance is a good place to start.

Table 4.3 Single jet propagation and detonability scaling tests. The listed yields are nuclear equivalents.

Test	Jet Geometry		Fuel Loading, lbm		Scale Factor	
	Diameter inches	Length ft	Jet	Hemisphere	Geometrical	Yield
15 ft hemisphere	0.125	15	0.083	50	1	1
20 ton hemisphere	0.543	65	6.8	4,100	4.34	82
100 ton hemisphere	0.93	112	34.2	20,500	7.42	410
50 lbm jet	1.05	127	50	-	8.43	600
Full-scale hemisphere	2.0	240	342	205,000	16.0	4100

SECTION 5

PRELIMINARY SPECIFICATIONS FOR NUCLEAR BLAST AND SHOCK SIMULATORS

The purpose of this section is to clarify some design issues involving four different types of blast and shock simulators. For underwater shock testing the range of nuclear weapons yields and overpressures that can be simulated with a limited energy source is addressed. For airblast testing, the ancillary effects of thermal fluence and dust lofting are considered. For the testing of both deep underground and shallow-buried structures the specification of the frequency passbands is established. The analyses are based on the use of extant data and first principles. Prior to looking at specific design problems the importance of establishing simulation criteria is discussed in Section 5.1.

5.1 SIMULATION CRITERIA

At the outset of a weapons effects simulation program it is prudent to address a half-dozen design issues that can have a significant impact on the ultimate usefulness of a simulator. The issues are set herein in the form of a series of questions whose answers will map out the region of usefulness of a simulator and establish guidelines for its use. To proceed, the six simulator design questions are posed as follows:

- (1) What is the environment to be simulated? The threat must be specified including weapon yield, burst location, and the effects of intervening media. For counter-attack planning the answers are fairly well set, but for defense planning the answers are uncertain.
- (2) How accurately is the environment known? Sophistication in design may be unwarranted if the environment is uncertain. Designing to bounding environments rather than average environments may be necessary. Most atmospheric nuclear tests were more concerned with weapons development than with gaining an understanding of the weapon produced environment. Moreover, for many applications structure loading levels have increased

to values that are not covered by data gathered many years ago. In many important cases the environment is not known accurately.

- (3) Does the environment itself have to be simulated or can the effects of the environment be simulated? For example, can the loading on a test structure be produced by high explosive detonation products instead of by airblast?
- (4) How sensitive is the response of the object to be tested to variations in the simulation parameters?
- (5) What are the differences between the weapon-produced environment and the simulated environment? In some cases the weapon produced environment is itself uncertain.
- (6) What is to be learned from the test?

The answers to these questions are important to ensure that the simulator design is technically correct, that the test results are valid, and that the design is economical. During the FAE feasibility program these questions should be addressed.

5.2 NUCLEAR UNDERWATER SHOCK EFFECTS

A 5-ms shock duration has been suggested for test purposes. This relatively short duration implies a shallow submerged depth for the test station. At depths where free surface cutoff does not play a role, the shock duration can be appreciably longer. The shock rise-time is sub-microsecond for overpressures in excess of 100 psig [25]. A simulator need not produce a fast rising shock, but must produce a pulse with a frequency spectrum sufficient to excite vibrational modes in a structure. The fundamental hoop period for a 10-meter diameter shell is approximately 6 ms. The problem in designing a simulator is not one of producing a fast rising pulse, but one of providing a long duration pulse.

The main issue addressed in this section is that of explosive weight limitation, imposed either by environmental or economic considerations, and the range of yields and overpressures that can be simulated by a limited weight of explosive. Conducting tests in a

sheltered area such as a harbor implies that the test duration will be short because of the shallow depth, and the test loading will be complicated because of bottom reflections. Some careful analysis is required. Deepwater testing, which allows for a long overpressure duration and large explosive weight is expensive. Minimization of explosive weight is a desirable goal. An energy balance can be used to relate the test waveform to the minimum energy required to drive a full scale test. To do so, the areal energy density in an overpressure wave of duration t is first calculated from

$$E/A = \int_0^t p u dt.$$

By approximating both the overpressure and particle velocity waves as exponentials in time at a fixed station and by relating the particle velocity to the overpressure through the acoustic impedance of seawater, Z , the areal energy density is given by,

$$E/A = \frac{p_o^2 \tau}{2Z} (1 - e^{-2t/\tau}),$$

$$E/A \doteq \frac{p_o^2 \tau}{2Z},$$

where p_o is the peak overpressure and τ is the e-folding time. The areal energy density is plotted in Figure 5.1 as a function of overpressure.

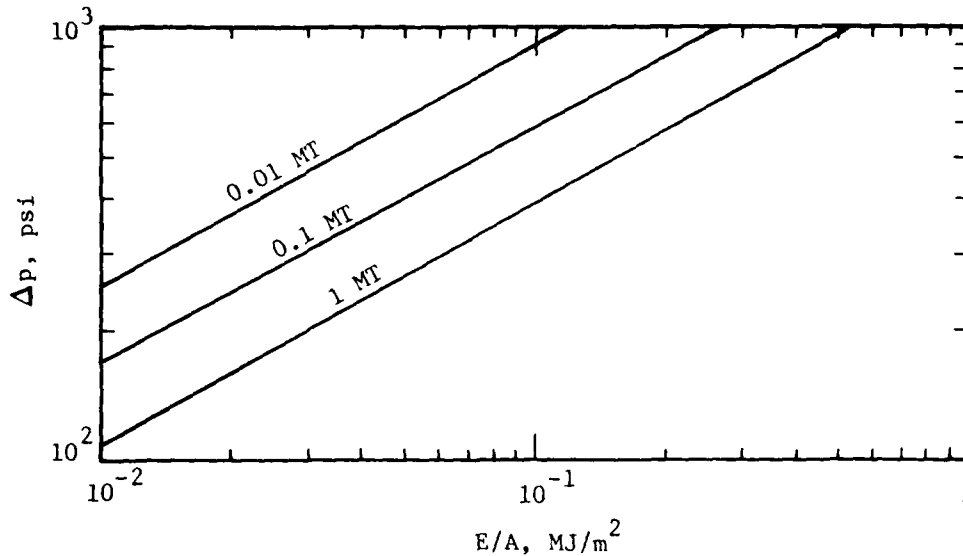


Figure 5.1 The areal energy density in a simulator overpressure wave as a function of overpressure level and weapon yield. An energy balance imposes a maximum overpressure and yield that can be simulated with a fixed quantity of energy assuming that all of the energy is focused on the target. Losses and finite geometry will reduce region accessible for simulation.

If a perfect simulator is assumed, which focuses all of its stored energy on the test station, then an upper bound can be placed on the overpressure and weapon yield that can be simulated for a deep-water attack with a fixed quantity of explosive. (An analogous calculation can be done for a shallow bottom or a shallow depth of explosion.) Losses and finite geometry will reduce the region accessible for simulation indicated in Figure 5.1, probably by more than a factor of ten in E/A which implies a factor of three reduction in overpressure for a fixed yield. The results suggest that if a focusing device could be devised it would allow a relatively small amount of explosive to simulate the effects of a large yield underwater explosion on a large target.

5.3 NUCLEAR AIRBLAST EFFECTS

An overpressure range of $1 \leq \Delta p \leq 100$ psig is adequate for testing a variety of unarmored battlefield equipment and reflects the FAE design. Armored equipment and strategic structures require an overpressure test ranging from several hundred psig to ten thousand psig. For defensive purposes yields are considered to lie in the range $0.01 \leq W \leq 25$ MT. The 10-KT lower limit appears to be a likely yield for a Soviet battlefield weapon. The inconsistency between the lower yield limit and a 1-KT FAE design for direct simulation testing must be resolved.

The 25-MT upper limit is as large as is usually considered in an attack scenario. Based on energy considerations, the use of three different simulators each with a ten-fold increase in maximum peak overpressure starting at 100 psi seems reasonable. The simulation of static and dynamic impulses from large yields (in excess of one to two kilotons) implies a directed energy source. The limits on the thermal fluence, Q , even for the 1- to 100-psi range and $0.01 \leq W \leq 1$ MT are quite wide, i.e., $2 < Q < 1000$ cal/cm². For $1 \leq \Delta p \leq 10,000$ psi and $0.01 \leq W \leq 25$ MT the thermal fluence is $2 \leq Q \leq 74,000$ cal/cm², Figure 5.2. The thermal fluence is calculated from [26,27]

$$Q = \frac{8.56 \times 10^4 f TW}{R^2} \text{ cal/cm}^2,$$

where f is the fraction of the weapon yield that contributes to thermal radiation, W is the yield in MT, R is the range in kft, and T is the transmission factor (plotted in References 25 and 26). For an airburst, f varies from 0.35 to 0.45 depending on yield and height of burst. The transmission factor varies, for example, from 0.9 to 0.01 for a clear day with 12-mile visibility and also depends on height of burst and range. For

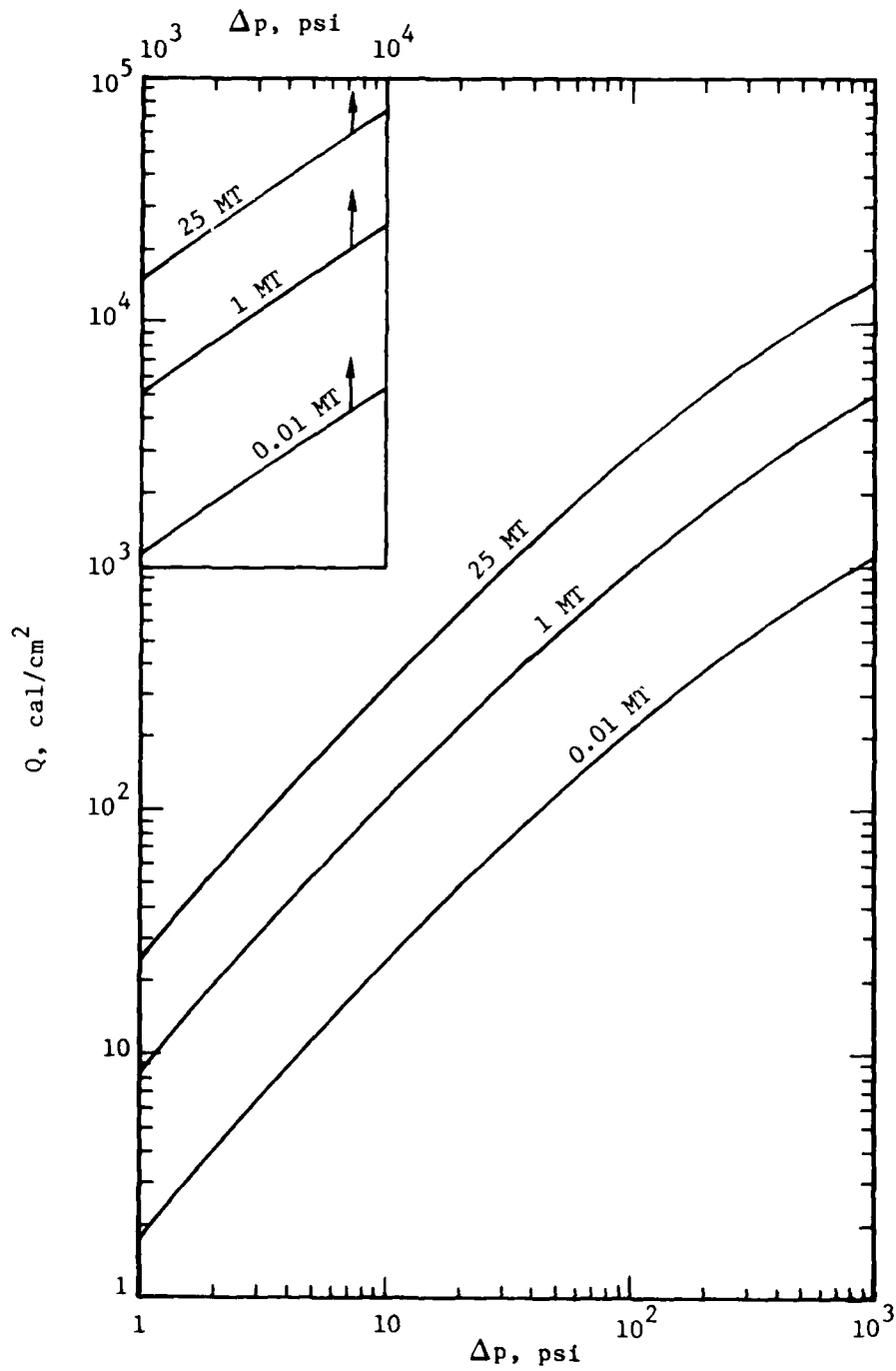


Figure 5.2 Thermal fluence vs overpressure and yield for a surface burst.

a surface burst, f is set equal to 0.18 to compensate for increased radiant absorption near the surface of the earth and standard height-of-burst transmission factors are used. For simplicity, T has been set equal to 0.8 in all of the calculations. This procedure results in the correct calculation of peak thermal fluences at the 100, 1,000, and 10,000 psig overpressure levels (which all occur at ranges less than 10,500 feet), but overestimates the fluence at ranges in excess of about 10,500 feet. The relation between overpressure and range was obtained by inverting Brode's formula [28],

$$R = \left\{ \frac{96W^{1/2}}{\Delta p} (1 + \sqrt{1 + 0.35807 \Delta p}) \right\}^{2/3}, \quad 2 \leq \Delta p \leq 10 \text{ psig}$$

which, for convenience, is plotted in Figure 5.3. Because of the offset between the U.S. '59 curve and Brode's calculation below 30 psig the U.S. '59 overpressure-range relation was used in plotting the thermal fluence below 30 psig. Failure to do so results in a 20-percent overestimate at the 1- to 2-psig level.

A dust density specification must distinguish between average densities and densities at altitude because the density of wind-lofted dust varies with the distance above the ground. Dust thrown up by thermal effects almost assuredly would show a similar gradient effect. The dust density, ρ_d , is of the order of $10^{-5} < \rho_d < 5 \times 10^{-3} \text{ gm/cm}^3$. Wind-lofted dust has been measured to have a density about equal to that of air near the surface of the ground [29]. For example, in controlled laboratory wind tunnel testing a 371-ft/s wind produced a dust density of $9.3 \times 10^{-4} \text{ gm/cm}^3$ six inches above the ground. Extrapolated to the ground surface, the dust density was $3.2 \times 10^{-3} \text{ gm/cm}^3$. Although the lofted particulate size distribution is nominally that of the in situ soil it is not unreasonable to expect that the distribution shifts to finer sizes with increasing altitude [30]. Crater lofted debris may include very large cobbles and boulders.

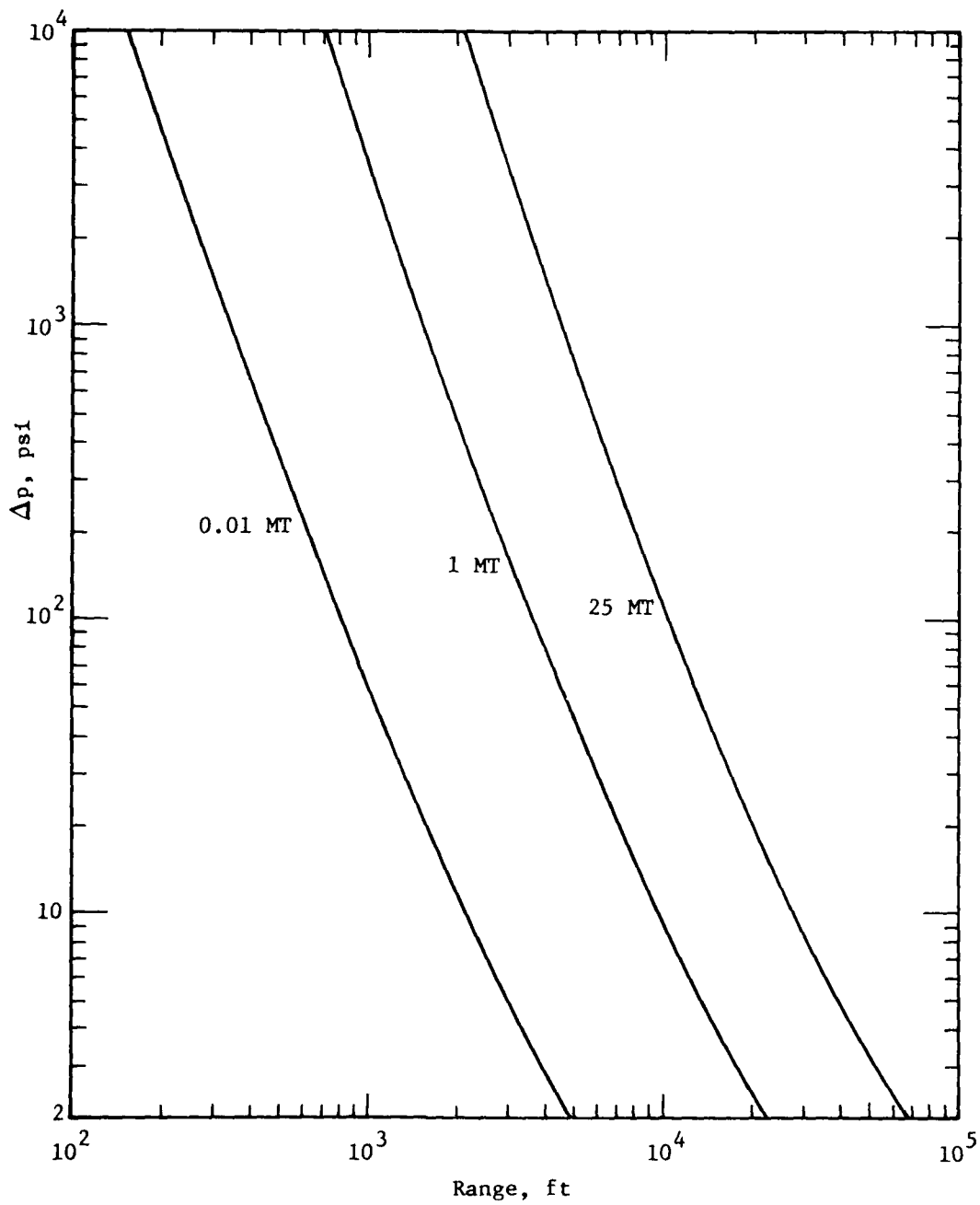


Figure 5.3. Range vs overpressure for surface bursts (Ref. 6).

5.4 DEEP BASED STRUCTURES

Based on the intrinsic strength of engineering materials a 2-kbar design is considered for a deep-based structure. Based on various attack scenarios, a 25-MT yield is considered. The main purpose of this section is to estimate the frequency content of the stress wave and this is done by using experimental data on stress wave rise time and pulse duration.

Because of the dispersive nature of geologic media the rise time of a stress wave depends on the distance that the wave has propagated. The relation between range and stress for a tamped explosion in hard rock is [31]

$$R = \frac{\sqrt{7} W^{1/3}}{\sqrt{\sigma}},$$

where R is in kft, W is in MT, and σ is in kbar. Although considerable uncertainty exists in determining the efficiency with which a surface burst or shallow-buried burst couples its energy into the ground, the ensuing calculations are based on a shallow-buried coupling efficiency of 0.16, so that

$$R = \frac{1.436W^{1/3}}{\sqrt{\sigma}}.$$

The high frequency cutoff of the stress wave is obtained from the rise time of velocity gauge signals. By using the rise time data compiled by Cooper [32] it is found that the fastest rise time of interest is 0.015 ± 0.008 seconds which corresponds to 2 kbar at 1020 feet from a 1-MT device. The longest rise time is 0.09 ± 0.045 seconds which corresponds to 0.5 kbar at 5940 feet from 25 MT. The upper and lower bounds on these rise times give frequencies of 46.7 and 2.6 Hz. Based on Piledriver data [33] in the 1- to 4-kbar range the positive phase of a 1-MT contained burst has a fundamental frequency of 1 Hz (about triple the positive phase frequency in air). A

25-MT burst produces a fundamental positive phase frequency of 0.3 Hz. (The uncertainty in stress levels arises from an inconsistency in Piledriver data: the velocity data imply a stress of 3.8 kbar while the stress records indicate 1.2 kbar. Velocity data are generally more reliable than stress data.)

To summarize, it is estimated that the frequency passband of a simulator which covers the range of yields, $1 \leq W \leq 25$ MT, and range of stress levels, $0.5 \leq \sigma \leq 2$ kbar, is no wider than $0.3 \leq f \leq 47$ Hz. For a given fixed yield and stress level the passband will be somewhat narrower, e.g., for $\sigma = 2$ kbar and $W = 1$ MT the low frequency limit is 1 Hz.

5.5 SHALLOW BURIED STRUCTURES

Based on proposed designs a 0.04-kbar lower limit on the peak stress is considered. The high frequency content of the stress wave is governed by the dispersive nature of the soil overburden while the low frequency content is controlled by weapon yield. For design purposes the air-blast induced rise time is given as [34]

$$t_r = 0.001 + \frac{z}{c_\ell} - \frac{z}{c_i} ,$$

where z is the depth of burial, c_ℓ is the speed of propagation of the peak stress, and c_i is the seismic speed. When wave speeds are not accurately known, c_ℓ is often set equal to one-half of c_i . For even modest depths of burial the rise time is controlled by the overburden. At the ground surface, $z = 0$, the rise time given by the formula is 1 ms, which raises a question about the accuracy of the data upon which the formula is based. With a 0.5-meter depth of burial and assuming $c_\ell = 350$ m/s, the high frequency cutoff is 146 Hz. At 1.0 meter depth of burial the frequency is

91 Hz. The fundamental frequency induced by the positive phase is as follows:

W, MT	p, psi	f, Hz
0.05	600	1.34
	10,000	0.90
0.01	600	2.29
	10,000	1.54
0.001	600	4.95
	10,000	3.33

Thus, the frequency passband of a simulator for shallow-buried structures which covers the range of yields, $0.001 < W \leq 0.05$ MT, the range of pressures $0.04 \leq \sigma \leq 0.70$ kbar, and the range of soil overburden $0.5 \leq d \leq 1.0$ meters is $0.9 \leq f \leq 146$ Hz.

SECTION 6

CONCLUSIONS AND RECOMMENDATIONS

An airblast simulator based on fuel-air explosives may circumvent some of the disadvantages attendant with using either solid explosives (TNT blocks or ANFO) or gaseous explosives (propane-oxygen or methane-oxygen), but a number of issues must be addressed to determine the feasibility of the FAE system. As with any system the FAE has its own potential problems and it is the size of these in relation to the defects of the other systems which must be quantified. The practicality of using fuel jets to create a detonable hemispherical fuel-air cloud has been demonstrated at small scale. The similarity between the airblast overpressure and stagnation pressure waveforms produced by a fuel-air explosion and by a nuclear explosion remains to be determined, both by careful blast measurements and accurate calculations.

The practicality of a full-scale FAE as currently envisioned depends heavily on the largely unknown propagation and dispersal characteristics of long-range liquid fuel jets. Calculations have indicated that long-range fuel jets can be used to create detonable mixtures, but the calculations are approximate, at best. Qualitative experiments have shown large differences between the propagation of a nonvolatile fluid (water) and a high vapor pressure fuel (propylene oxide), an effect not accounted for in existing theories. Scaling laws have not been uncovered to relate the dispersal of fuel in a full-scale jet, with a reach in excess of 235 feet, to that of the small-scale jet, with a reach of 15 feet, used in the hemispherical detonation studies, making the scale-up of the FAE uncertain. Emphasis must be placed on experiments to produce long range, detonable fuel jets and to understand how the FAE dispersal techniques and detonation depend upon scale. Both propylene oxide and lower cost fuels should be examined.

A major problem is involved in determining the size of the next generation of hemispherical FAE experiments. Based on the extant work on jets and fuel-air detonations, it appears that the conventional engineering

approach of scaling-up in steps should be used and that an intermediate size test facility should be constructed prior to a full-scale facility.

The existence of blast irregularities, either asymmetries or multiple wave effects, arising from possible inhomogeneous fuel dispersal is a concern that must be investigated by careful blast measurements on the small-scale FAE system.

Simulation criteria, not only for airblast, but also for underwater shock and ground shock need to be formulated to guide simulator development and usage. For example, the contemplated full scale FAE design is based upon current simulator practices, but there is concern about the relatively small yield in relation to the perceived threat and the scale at which testing is performed.

SECTION 7

REFERENCES

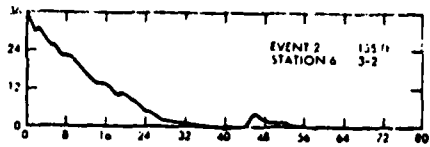
1. Reisler, R., and Ethridge, N., "Airblast Overpressure Phenomena," Operation Distant Plain Symposium, DASA 1947-1, Sept. 1967, pp. 42-85.
2. Pattman, A. and Anderson, J., "Canadian Air Blast Measurements in Operation Distant Plain," Operation Distant Plain Symposium, DASA 1947-1 Sept. 1967, pp. 118-134.
3. Balcerzak, M., Johnson, M. and Lucole, S., Nuclear Blast Simulation - Detonable Gas Explosion - Operation Distant Plain, DASA 1945, April 1967.
4. Brode, H., "Review of Nuclear Weapons Effects," Annual Review of Nuclear Science, Vol. 18, 1968, pp. 153-202.
5. Glasstone, S. and Dolan, P., The Effects of Nuclear Weapons, 3rd edition, U.S. Dept. of Defense and U.S. Dept. of Energy, 1977
6. Needham, C., Havens, M., and Knauth, C., Nuclear Blast Standard (1 KT), AFWL-TR-73-55 (Rev.), April 1975.
7. Brode, H., "Blast Wave from a Spherical Charge," Physics of Fluids, Vol. 2, No. 2, March-April 1959, pp. 217-229.
8. Ibid.
9. Balcerzak, M., "Detonable Gas Explosion," Operation Distant Plain Symposium, DASA, 1947-1, Sept. 1967, p. 211.
10. Brode, H. "Review of Nuclear Weapons Effects," Annual Review of Nuclear Science, Vol. 18, 1968, pp. 153-202.
11. Pattman, A. and Anderson, J., loc. cit.
12. Brode, H., "Blast Wave form a Spherical Charge," Physics of Fluids, Vol. 2, No. 2, March-April 1959, pp. 217-229.
13. Benedick, W., personal communication.
14. Phinney, R., Breakup of a Turbulent Jet in a Low-Pressure Atmosphere, AICHE Journal, 21, No. 5, pp. 996-999, Sept. 1975.
15. Abramovich, The Theory of Turbulent Jets, MIT Press, 1963.
16. Townsend, A., Fluid Mech. 26, 1966, p. 689.

17. Phinney, R., loc. cit.
18. Hartenbaum, B., Lofting of Particulates by a High Speed Wind, DNA 2737, Sept. 1971.
19. Alger, T. and Giedt, W., A Light Scattering Technique for Determining Droplet Size Distribution in Two-Phase Liquid Dominated Nozzle Jets, Lawrence Livermore Laboratory, Jan. 1978, UCRL-79647.
20. Benedick, W., personal communication.
21. Phinney, R., loc. cit.
22. Fire Protection Handbook, 14th edition, National Fire Protection Association, 1976.
23. Sedgwick, R., Kratz, H., and Herrmann, R., Feasibility Investigation of a Permanent Fuel-Air Explosive Blast Simulator, Systems, Science and Software Report SSS-R-78-3737, August 1978.
24. Glasstone, S., loc. cit.
25. Cole, R., Underwater Explosions, Dover, New York, 1965.
26. Crawford, R., Higgins, C., and Bultman, E., The Air Force Manual for Design and Analysis of Hardened Structures, AFWL-TR-74-102, Oct. 1974.
27. Glasstone, S., loc. cit.
28. Brode, H., "Review of Nuclear Weapons Effects," Annual Review of Nuclear Science, Vol. 18, 1968.
29. Hartenbaum, B., loc. cit.
30. Leese, G. and Vedros, P., Dust Cloud Sampling During Operation Distant Plain, U.S. Army Waterway Experiment Station Miscellaneous Paper No. 4-977, March 1968.
31. Cooper, H., Empirical Studies of Ground Shock and Strong Motions in Rock, RDA-TR-3601-002, Oct. 1973.
32. Ibid.
33. Perret, W. and Bass, R., Free Field Ground Motion Induced by Underground Explosions, SAND74-0252, Feb. 1975.
34. Crawford, R., Higgins, C. and Bultmann, loc. cit.

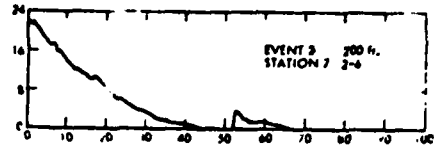
APPENDIX A
NOMENCLATURE

A	area
D	initial diameter of jet
E	energy
L	length of jet
p	pressure
Q	thermal fluence
r	jet radius
r_o	initial jet radius
R	range
u	jet velocity
W	energy
We	Weber number = $\rho_l u^2 D / \sigma$
x	axial distance along jet
x_n	location of jet transition section
x_o	apparent point source of jet
y	radial position
Z	acoustic impedance
ρ_a	density of air
ρ_l	density of liquid
σ	surface tension
τ	time constant
X	fuel concentration
$()_m$	value on jet axis
$()_o$	peak value

APPENDIX B
OVERPRESSURE WAVEFORMS

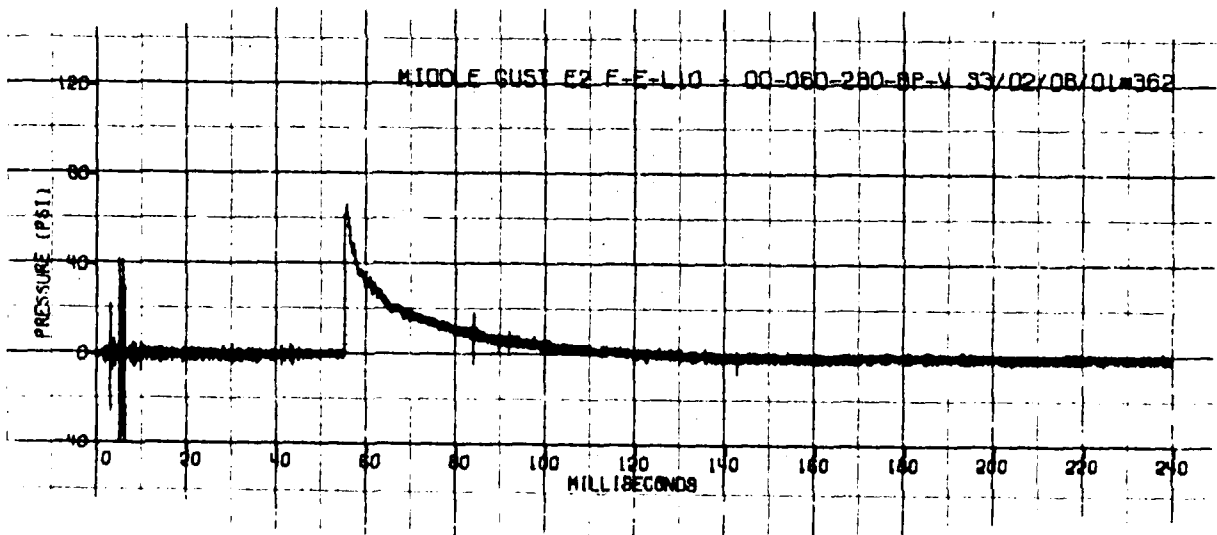


(a) 155 ft



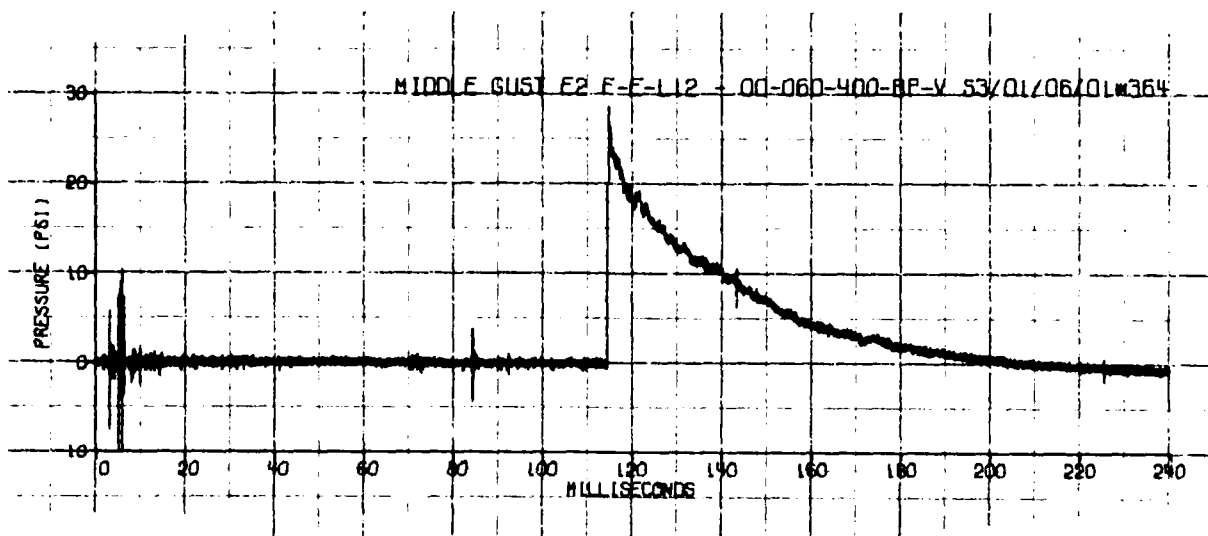
(b) 200 ft

Distant Plain 2a



(a) 280 ft

MIDDLE GUST II



(b) 400 ft

MIDDLE GUST II

DISTRIBUTION LIST

DEPARTMENT OF DEFENSE

Assistant to the Secretary of Defense
Atomic Energy
ATTN: Executive Assistant

Defense Advanced Rsch. Proj. Agency
ATTN: TIO

Defense Intelligence Agency
ATTN: DT-1C
ATTN: DB-4C, E. O'Farrell
ATTN: DT-2

Defense Nuclear Agency
ATTN: SPAS
ATTN: DDST
ATTN: SPTD
2 cy ATTN: SPSS
4 cy ATTN: TITL

Defense Technical Information Center
12 cy ATTN: DD

Department of Defense Explo. Safety Board
ATTN: Chairman

Field Command
Defense Nuclear Agency
ATTN: FCTMOF
ATTN: FCT
ATTN: FCPR

Field Command
Defense Nuclear Agency
Livermore Division
ATTN: FCPRL

Field Command Test Directorate
ATTN: FCTC

NATO School, SHAPE
ATTN: U.S. Documents Officer

Undersecretary of Def. for Rsch. & Engrg.
ATTN: Strategic & Space Systems (OS)

DEPARTMENT OF THE ARMY

Chief of Engineers
Department of the Army
ATTN: DAEN-RDM
ATTN: DAEN-MCE-D

Deputy Chief of Staff for Ops. & Plans
Department of the Army
ATTN: MOCA-ADL

Harry Diamond Laboratories
Department of the Army
ATTN: DELHD-N-P
ATTN: DELHD-I-IL

U.S. Army Material & Mechanics Rsch. Ctr.
ATTN: Technical Library

DEPARTMENT OF THE ARMY (Continued)

U.S. Army Ballistic Research Labs.
ATTN: DRDAR-BLT, W. Taylor
ATTN: DRDAR-TSB-S
ATTN: DRDAR-BLE, J. Keefer
ATTN: DRDAR-BLV

U.S. Army Engr. Waterways Exper. Station
ATTN: Library
ATTN: WESSD, G. Jackson
ATTN: WESSA, W. Flathau
ATTN: J. Strange

U.S. Army Materiel Dev. & Readiness Cmd.
ATTN: DRXAM-TL

U.S. Army Missile Command
ATTN: RSIC

U.S. Army Mobility Equip. R&D Cmd.
ATTN: DRDME-WC

U.S. Army Nuclear & Chemical Agency
ATTN: Library

DEPARTMENT OF THE NAVY

David Taylor Naval Ship R&D Ctr.
ATTN: Code 17
ATTN: Code L42-3
ATTN: Code 1844
2 cy ATTN: Code 1740.5, B. Whang

Naval Construction Battalion Center
ATTN: Code L51, R. Odello
ATTN: Code L08A

Naval Electronic Systems Command
ATTN: PME 117-21

Naval Facilities Engineering Command
ATTN: Code 04B
ATTN: Code 09M22C
ATTN: Code 03T

Naval Material Command
ATTN: MAT 08T-22

Naval Research Laboratory
ATTN: Code 8440, G. O'Hara
ATTN: Code 2627

Naval Sea Systems Command
ATTN: SEA-0351
ATTN: SEA-09G53
ATTN: SEA-322

Naval Surface Weapons Center
ATTN: Code F31
ATTN: Code R14, T. Blatstein
ATTN: Code R14

Naval Surface Weapons Center
ATTN: Tech. Library & Info. Services Branch

DEPARTMENT OF THE NAVY (Continued)

Office of Naval Research
ATTN: Code 474, N. Perrone
ATTN: Code 715

Office of the Chief of Naval Operations
ATTN: OP 03EG
ATTN: OP 981

Strategic Systems Project Office
Department of the Navy
ATTN: NSP-43
ATTN: NSP-272

DEPARTMENT OF THE AIR FORCE

Air Force Geophysics Laboratory
ATTN: LWV, K. Thompson

Air Force Institute of Technology
ATTN: Library

Air Force Systems Command
2 cy ATTN: DLW

Air Force Weapons Laboratory
Air Force Systems Command
ATTN: DES-C, R. Henny
ATTN: SUL
ATTN: DEX
ATTN: DE, M. Plamondon

Assistant Chief of Staff
Intelligence
Department of the Air Force
ATTN: TNT

Deputy Chief of Staff
Research, Development, & Acq.
Department of the Air Force
ATTN: AFRDQSM

Strategic Air Command
Department of the Air Force
ATTN: NRI-STINFO, Library

DEPARTMENT OF ENERGY

Department of Energy
Albuquerque Operations Office
ATTN: CTID

Department of Energy
ATTN: Document Control for OMA/RD&T

Department of Energy
Nevada Operations Office
ATTN: Mail & Records for Technical Library

DEPARTMENT OF ENERGY CONTRACTORS

Lawrence Livermore Laboratory
ATTN: Document Control for L-96, L. Woodruff
ATTN: Document Control for Tech. Info. Dept. Lib.

Los Alamos Scientific Laboratory
ATTN: Document Control for MS 364

Sandia Laboratories
ATTN: Document Control for 3141

DEPARTMENT OF ENERGY CONTRACTORS (Continued)

Sandia Laboratories
ATTN: Document Control for Lib. & Sec. Class.
Div.

OTHER GOVERNMENT AGENCY

Federal Emergency Management Agency
ATTN: Hazard Eval. & Vul. Red. Div., G. Sisson

DEPARTMENT OF DEFENSE CONTRACTORS

Aerospace Corp.
ATTN: Technical Information Services

BDM Corp.
ATTN: Corporate Library
ATTN: T. Neighbors

Boeing Co.
ATTN: Aerospace Library

California Research & Technology, Inc.
ATTN: M. Rosenblatt

California Research & Technology, Inc.
ATTN: D. Orphal

Civil Systems, Inc.
ATTN: J. Bratton

EG&G Washington Analytical Services Center, Inc.
ATTN: Library

Eric H. Wang
Civil Engineering Rsch. Fac.
ATTN: N. Baum

General Electric Co.—TEMPO
ATTN: DASIAC

Geocenters, Inc.
ATTN: E. Marram

H-Tech Labs., Inc.
ATTN: B. Hartenbaum

IIT Research Institute
ATTN: Documents Library

Institute for Defense Analyses
ATTN: Classified Library

JAYCOR
ATTN: H. Linnerud

Kaman Sciences Corp.
ATTN: Library

Lockheed Missiles & Space Co., Inc.
ATTN: T. Geers
ATTN: Technical Library

Lockheed Missiles & Space Co., Inc.
ATTN: TIC-Library

Lovelace Biomedical & Environmental Rsch. Inst., Inc.
ATTN: D. Richmond

DEPARTMENT OF DEFENSE CONTRACTORS (Continued)

Merritt CASES, Inc.
ATTN: J. Merritt

University of New Mexico
ATTN: CERF, G. Leigh
ATTN: CERF, N. Baum

Pacifica Technology
ATTN: J. Kent

Physics International Co.
ATTN: F. Moore
ATTN: Technical Library
ATTN: F. Sauer

R & D Associates
ATTN: J. Lewis
ATTN: C. MacDonald
ATTN: Technical Information Center
ATTN: R. Port

Physics Applications, Inc.
ATTN: F. Ford

Science Applications, Inc.
ATTN: Technical Library

Science Applications, Inc.
ATTN: J. Dishon

DEPARTMENT OF DEFENSE CONTRACTORS (Continued)

Science Applications, Inc.
ATTN: M. Knasel

Southwest Research Institute
ATTN: W. Baker
ATTN: A. Wenzel

SRI International
ATTN: G. Abrahamson
2 cy ATTN: B. Gasten

Systems, Science & Software, Inc.
ATTN: D. Grine
ATTN: Library
ATTN: R. Sedgwick
ATTN: T. Pierce

TRW Defense & Space Sys. Group
ATTN: D. Baer
ATTN: Technical Information Center
2 cy ATTN: P. Dai

TRW Defense & Space Sys. Group
ATTN: E. Wong

Weidlinger Assoc., Consulting Engineers
ATTN: M. Baron

Weidlinger Assoc., Consulting Engineers
ATTN: J. Isenberg